Cognitive and neural mechanisms underlying sequential risk-taking behaviors among individuals with internet gaming disorder

Abstract

Background: Internet Gaming Disorder (IGD) is one type of behavioral addiction characterized by compulsive internet gaming despite negative consequences. Understanding the cognitive and neural mechanisms underlying decision-making in individuals with IGD is essential to address this growing mental health concern. This study investigates risky decision-making behaviors and their neural correlates in individuals with IGD compared to healthy controls (HCs).

Methods: A total of 42 right-handed participants, including 15 with IGD and 27 HCs, underwent a sequential risk-taking task. Behavioral data were collected and analyzed using computational models to assess risk-taking propensity influenced by emotional responses. Concurrent functional near-infrared spectroscopy (fNIRS) and electroencephalography (EEG) recordings allowed for the assessment of neural activity during decision-making.

Results: In sequential risky taking decision-making, both IGDs and HCs showed a greater risky propensity after negative outcomes than positive outcomes. Meanwhile, individuals with IGD exhibited a higher risk-taking propensity compared to the HC group, as determined by computational modeling. EEG analysis identified significant differences in univariate pattern analysis, like global field power, event related potential, and Multivariate pattern analysis between IGD and HC groups in response to win and loss feedback. In addition, significant brain deactivation alternation in the prefrontal cortex during the task was detected for the patient group compared with that from the control group.

Conclusions: Risky decision-making in IGD appears to be influenced by complex interactions between emotional responses and cognitive factors. The findings offer a foundation for understanding the aberrant

decision-making processes in IGD and may inform future interventions and treatments for this behavioral addiction.

Keywords: Risky decision making; Internet gaming disorder; Computational modeling; EEG; functional near infrared spectroscopy.

Introduction

The Internet Gaming Disorder (IGD) represents a prominent form of behavioral addiction, characterized by repetitive and compulsive engagement in internet gaming activities without considering the negative consequences (Derevensky, Hayman, & Lynette, 2019). Given its high prevalence rates, ranging from 0.21% to 57.50% in general populations worldwide (Stevens, Dorstyn, Delfabbro, & King, 2021), IGD has emerged as a significant mental health concern and been included in both the 11th revision of the International Classification of Diseases (ICD-11) and the fifth edition of the Diagnostic and Statistical Manual of Mental Disorders (DSM-5) (Luo, Wei, Guo, Hu, Chao, Sun et al., 2021). Similar to substance use disorder, IGD has been associated with dysfunctions in dopaminergic neural circuitry involved in compulsive seeking of sensation, prefrontal cortex dysfunction related to impulsive control, and amygdala involvement in negative emotional reactions (Weinstein & Lejoyeux, 2020). These neurobiological alterations suggest that IGD shares similarities with psychiatric disorders including major depressive disorder, anxiety, and attention deficit hyperactivity disorder (Ko, Yen, Yen, Chen, & Chen, 2012; Ostinelli, Zangani, Giordano, Maestri, Gambini, D'Agostino et al., 2021). Furthermore, previous research has indicated impaired response inhibition, emotion dysregulation, and deficits in working memory among individuals with IGD using neurocognitive tasks (Argyriou, Davison, & Lee, 2017; Shin, Kim, Kim, & Kim, 2021; Z. Zhou, Zhou, & Zhu, 2016). However, the potential neural mechanisms underlying IGD and the specific cognitive impairments in complex cognitive processes, such as decision-making, remain largely unknown.

In particular, impaired decision-making, characterized by a propensity for risky behavior and irrational delay-counting, is considered as a core feature of several neuropsychiatric disorders (Zeng, Tang, Gao, Tang, Zhang, Zhang et al., 2023). Decision-making is a crucial cognitive process involving the evaluation of alternative outcomes in terms of desirability and probability (Rilling & Sanfey, 2011). It can be categorized into two types: ambiguity decision-making and risky decision-making, depending on whether the probabilities of outcomes are predictable (Y. Li, Chen, Zhang, Turel, Bechara, Feng et al., 2019). In risky decision-making, for instance, even when the outcome probabilities are known, decision-making behavior is influenced by various factors, including valence of outcomes (win/lose), amplitude and probability of cost-benefit, characteristics of participants (e.g., risky propensity and inverse temperature), emotional regulation, among others (Kusev, Purser, Heilman, Cooke, Van Schaik, Baranova et al., 2017). Specifically, previous studies have demonstrated that outcomes can significantly influence subsequent decision-making patterns (Figner, Mackinlay, Wilkening, & Weber, 2009; Oskarsson, Van Boven, McClelland, & Hastie, 2009). For example, participants displayed increased risk-seeking behavior following a loss in risk decision-making paradigms (Z. Liu, Cheng, Liu, Zhang, Li, Li et al., 2020; Xue, Lu, Levin, & Bechara, 2011). Conversely, Pedroni, Gianotti, Koenig, Lehmann, Faber, and Knoch (2017) found that participants exhibited greater risk-taking tendencies after experiencing wins, a phenomenon known as positive recency in sequential decision-making paradigms. For now, it remains unclear whether positive or negative outcomes from the previous trial would promote or impede risk-taking behaviors.

Existing findings on the behaviors of IGD in risky decision-making were rather mixed (Y.-W. Yao, Zhang, Fang, Liu, & Potenza, 2022). Some studies reported no group difference of risky propensity between individuals with IGD and health controls (HCs) (Deleuze, Nuyens, Rochat, Rothen, Maurage, & Billieux, 2017; Y. W. Yao, Chen, Li, Wang, Zhang, Yip et al., 2015). By contrast, individuals with IGD were also found to exhibit reduced loss aversion and make riskier choices in the loss domain (Y. W. Yao, Chen et al., 2015), while participants with IGD made riskier choices in the gain domain (Ko, Wang, Liu,

Chen, Yen, & Yen, 2017). These findings suggested that the risky propensity of individuals with IGD may be modulated by some confounding factors. Specifically, no studies have explored whether IGD manifests different behavioral patterns influenced by the valence of the previous trial (win or loss outcome). Thus, to better evaluate the affecting factors in risky propensity, this study aims to examine the effects of outcome valence on subsequent decision-making performance in individuals with IGD using a sequential risk-taking paradigm (Brassen, Gamer, Peters, Gluth, & Büchel, 2012).

Besides, decision-making behavior is influenced by various factors including loss aversion and risk propensity. As conventional behavioral data analysis may not capture these nuanced characteristics, computational modeling of cognitive tasks has been widely employed in clinical populations to overcome the limitations of traditional behavioral tasks. Previous studies constructed computational models to reflect individual learning ability, sensitivity to wins and losses, inverse temperature, and risk-taking propensity in sequential risky decision making such as the Balloon Analogue Risk Task (BART) (H. Park, Yang, Vassileva, & Ahn, 2021; van Ravenzwaaij, Dutilh, & Wagenmakers, 2011; R. Zhou, Myung, & Pitt, 2021). Yet, we used a sequential risk-taking paradigm instead of BART for the current study, as participants need to extra learn the probability of balloon pumping in BART. As such, we would utilize modified models to the potential risk-taking propensity and behavioral consistency during the task.

Furthermore, to investigate the potential neural mechanisms of IGD in sequential risky decision-making, we will employ functional near-infrared spectroscopy (fNIRS) neuroimaging and electrophysiology (EEG) simultaneously. The combination of EEG and fNIRS would provide valuable insights into the neural dynamics underlying decision-making, as they capture event-related potentials (ERPs), brain oscillation characteristics, and oxygenated hemoglobin (HbO) concentration changes of perceiving outcomes, during decision making process (Fei Gao, Hua, He, Xu, Li, Zhang et al., 2023; F. Gao, Wang, Armada-da-Silva, Wang, Lu, Leong et al., 2022; R. Li, Yang, Fang, Hong, Reiss, & Zhang, 2022). Previous studies have reported abnormal activation in the prefrontal cortex (PFC) of individuals with IGD using functional

Magnetic Resonance Imaging and the BART (L. Liu, Xue, Potenza, Zhang, Yao, Xia et al., 2017; Qi, Du, Yang, Du, Gao, Zhang et al., 2015), Thus, fNIRS will be used to measure changes in HbO concentration in the PFC during sequential risky decision-making. In addition, studies utilizing brain electrophysiological activities have found higher brain oscillations in slow-wave activity (theta, beta) among individuals with IGD (Y. J. Kim, Lee, Oh, Park, Jung, Sohn et al., 2017) and observed differences in feedback-related negativity (FRN) and P300 amplitudes in risk decision-making tasks (Q. Li, Wang, Yang, Dai, Zheng, Sun et al., 2020; Yau, Potenza, Mayes, & Crowley, 2015; Zhao, Li, Hu, Wu, & Liu, 2017). Especially, compared to univariate pattern analysis (ERPs), the multi-variates pattern analysis (MVPA) can decode neural activities across multiple EEG channels, with enhanced sensitivity, integrated information, reduced the noise influence, etc (Grootswagers, Wardle, & Carlson, 2017). In light of the MVPA strength and no previous studies have adopted this technique to decode the neural activity of perceiving feedbacks, we wish to explore the different time course of potential neural activity perceiving the valence of feedbacks among IGD and HCs.

Therefore, this study aims to investigate the behaviors and related neural mechanisms underlying sequential risk-taking among individuals with IGD and HCs. We hypothesize that individuals with IGD will exhibit riskier behaviors compared to HCs and that the valence of the previous trial will further influence subsequent risk-taking behaviors. To test this hypothesis, we will employ a combination of behavioral modeling and EEG-fNIRS fusion neuroimaging to systematically characterize specific impairments and potential neural mechanisms during a sequential risk-taking task. The computational modeling approach will provide insights into the nuanced cognitive processes involved in sequential risk-taking, contributing to a better understanding of the abnormalities underlying aberrant risky decision-making performance. Furthermore, the combination of EEG and fNIRS will provide a multi-dimensional view of the neural mechanisms underlying decision-making, capturing both millisecond-level neural activity (EEG) and the hemodynamic response (fNIRS).

2 Method

2.1 Participants

A total of 42 right-handed participants, including 15 individuals with IGD (mean age: mean age: 21.46, 6 females) and 27 health controls (HC, mean age: 21.67, 17 females), were recruited from the University of Macau. The inclusion criteria for IGD were as follows: 1) aged between 20 and 30 years with more than 12 years of education; 2) played internet games for at least 4 hours per day on weekdays and 8 hours per day on weekends, or a total of 40 hours per week, for a minimum duration of 2 years, as confirmed by total game time records. Participants in the control group were gender-, age-, and education-level matched with those in the IGD group and had a nonessential internet use of less than 4 hours per day in their daily lives. A semi-structured interview was conducted to assess the DSM-5 criteria for IGD, and participants needed to fulfill at least five out of nine items as defined by the DSM-5 definition (Luo, Wei et al., 2021). All individuals with IGD completed the Chen Internet Addiction Scale (CIAS) (Chen, Weng, Su, Wu, & Yang, 2003). Together, CIAS and DSM-5 were used to indicate the severity of internet addiction. The Barratt Impulsiveness Scale (BIS-11), a widely used assessment of impulsiveness, was administered to all participants (X.-y. Li, Phillips, Xu, Zhang, Yang, Tong et al., 2011). Informed consent was obtained from all participants prior to the experiment, and the protocol and procedures of this study were approved by the Institutional Review Board of the University of Macau.

2.2 Procedure

Participants were seated in a quiet room where both behavioral data and EEG-fNIRS signals were recorded simultaneously during the task. Before the formal experiment, participants were instructed to aim to obtain as many rewards as possible during the task, which were associated with their final

payments. Initially, participants practiced the task for 16 trials to ensure they understood the procedures. Following the practice session, participants were instructed to rest for one minute as a baseline period. Then, participants performed 200 formal trials, which took approximately 30-40 minutes to complete.

Each trial consisted of four phases: fixation, decision-making, feedback, and rating (Figure 1). After the presentation of a fixation cross lasting for 1-3 seconds, eight closed boxes were presented on the computer screen, of which 7 contained gains (gold) and one contained a loss (devil). The position of loss was randomly assigned to one of the eight boxes. The boxes were sequentially opened from left to right. At each position, participants had to decide whether to open the next box or stop here and collect the gains acquired so far in that trial by pressing a key within 2000 ms. If no response was made within the time limit, the boxes would be opened automatically. The decision-making phase ended when the box containing the loss was opened (defined as the lose condition) or when participants chose to stop (defined as the gain condition) before opening all the boxes. The feedback phase lasted for 3000 ms and indicated whether the participant won or lost for that trial. The screen also displayed the actual position of the loss, informing participants about the points they had collected and the chances they had missed. Finally, participants were asked to rate their feelings about their choice and the outcomes of the trial on a 9-point scale ranging from extreme regret (defined as -4) to extreme relief (defined as 4).

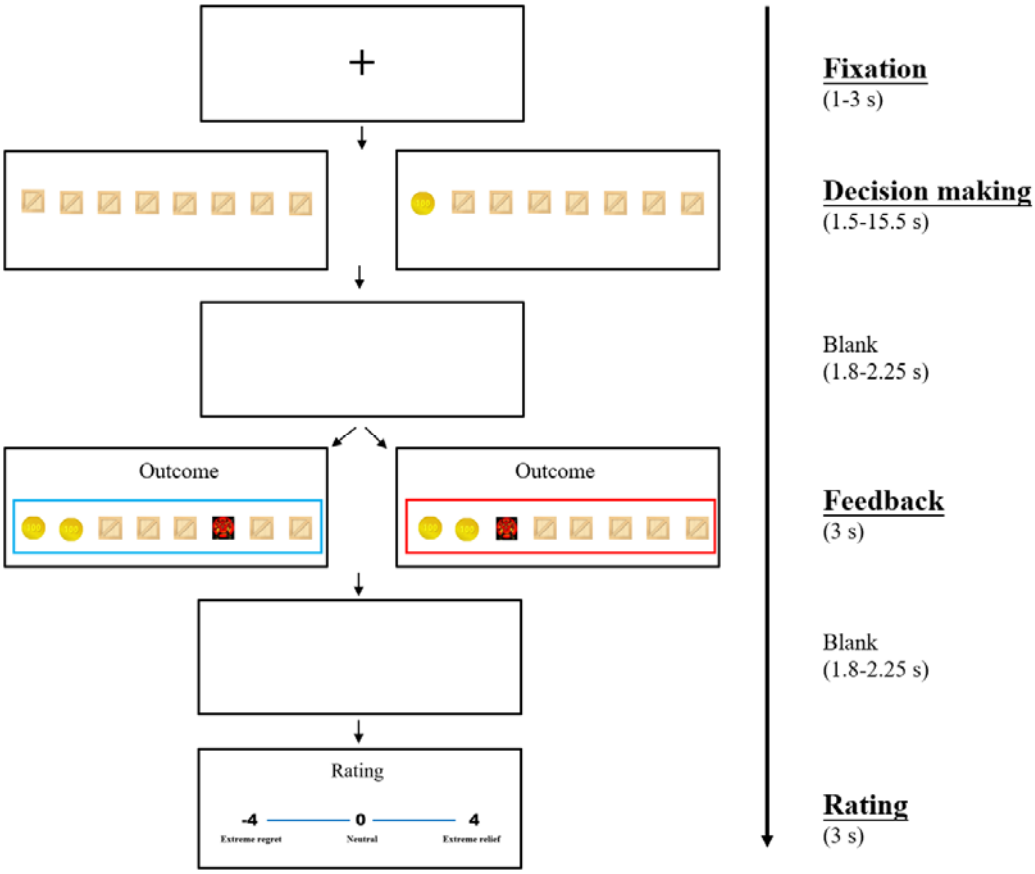

Fig. 1. Schematic of the sequential risk-taking task. The trial of sequential risk-taking task was composed of fixation period, decision making period, feedback presentation period and rating period.

2.3 Behavioral modelling

2.3.1 Model details

As the procedure mentioned earlier, the probability of meeting devils (losing the coins of that trial) p_k^{lose} is 1/8. Thus, according to van Ravenzwaaij, Dutilh et al. (2011), the expected utility after l boxes on trial k, U_{kl} can be presented as:

$$U_{kl} = (1 - p_k^{loss})^l * l^\gamma with\ \gamma\ \geq 0 \quad (2)$$

the optimal boxes opened (v_k) can be calculated by setting the first derivative of Eq. (4) for l equals zero. Here we can get the optimal boxes opened:

$$v_k = \frac{-\gamma}{\ln(1 - p_k^{loss})}\ with\ \gamma\ \geq 0 \quad (3)$$

Considering the randomness trait of decision making, here we use the parameter τ, to present inverse temperature of participants, in which higher τ value indicates more deterministic behavior of the decision making. So, we could calculate the probability p_{kl}^{open} if the participants opened the boxes l on trial k.

$$p_{kl}^{open} = \frac{1}{1 + e^{\tau(l - v_k)}}\ with\ \tau\ \geq 0 \quad (4)$$

Considering that the behaviors in the next trial would be influenced by the emotional response of previous trial, here we proposed a revised model (parameter-3 model). In this model, we used a parameter a to present the degree of the participants being influenced by emotional response of last trial. Thus, the probability p_{kl}^{open}, can be rewritten as:

$$p_{kl}^{open} = \frac{1}{1 + e^{\tau*(l - v_k)*a*er_{k-1}}}\ with\ \tau\ \geq 0 \quad (5)$$

The er_{k-1} is the emotional rating scores in last trial.

2.3.2 Parameter Estimation

The parameters of the two computational models were estimated through a hierarchical Bayesian analysis framework, as outlined by Lee (2011). This approach enables the simultaneous estimation of both individual and group-level data in a mutually constraining manner. The implementation of hierarchical Bayesian analysis utilized the Stan software package (https://mc-stan.org/) and the hBayesDM package (Ahn, Haines, & Zhang, 2017) within the R programming environment (http://www.r-project.org/). We

employed the Hamiltonian Monte Carlo method to facilitate the estimation process. To ensure convergence to the desired distributions, a substantial sample size of 4000 was employed. Additionally, we ran four independent chains to assess whether the posterior distributions remained independent of the initial starting points. This rigorous approach was designed to enhance the robustness and reliability of our parameter estimates.

2.3.3 Model Comparison

The performance of the two models was compared using the leave-one-out information criterion (LOOIC) (Vehtari, Gelman, & Gabry, 2017). LOOIC was calculated based on leave-one-out cross-validation, estimating out-of-sample prediction accuracy from the log-likelihood derived from the posterior distributions. A lower LOOIC score indicates a better model performance. LOOIC weights, defined by Akaike weights (Wagenmakers, Farrell, & review, 2004) based on LOOIC values, were used to compare the models.

$$w_i(LOOIC) = \frac{\exp\left\{-\frac{1}{2}\Delta_i(LOOIC_i - LOOIC_{\min})\right\}}{\sum_{n=1}^{N}\exp\left\{-\frac{1}{2}\Delta_n(LOOIC_i - LOOIC_{\min})\right\}} \quad (6)$$

2.4 Concurrent fNIRS and EEG recordings

Participants wore a fused fNIRS-EEG data acquisition cap (EasyCap, Herrsching, Germany) with reference to the international 10-20 system to enable concurrent fNIRS and EEG acquisition. The fNIRS data were collected using the NIRScout system (NIRx Medizintechnik GmbH, Berlin, Germany), which had 8 LED sources and 8 detectors, resulting in 20 measurement channels with an inter-optode distance of 30 mm along the bilateral frontal regions. The light attenuation was measured at wavelengths of 760 nm and 850 nm at a sampling rate of 7.81 Hz. The Montreal Neurological Institute (MNI) coordinates of each fNIRS channel were quantified using the ICBM-152 head model (Singh, Okamoto, Dan, Jurcak, & Dan,

2005) and the NIRSite 2.0 toolbox (NIRx Medizintechnik GmbH, Berlin, Germany), listed in Table 1. These coordinates were then imported into the NIRS-SPM software toolbox for spatial registration (Ye, Tak, Jang, Jung, & Jang, 2009).

EEG data were recorded using 32 Ag/AgCl active electrodes (Brain Products, Munich, Germany) attached to the EEG cap (sampling rate: 500 Hz, bandpass: 0.03-70 Hz, reference: Cz). Due to the placement of fNIRS probes, five EEG electrodes were relocated to neighboring channels (Figure 2A). The impedance of each channel was maintained below 25 kΩ before concurrent data acquisition.

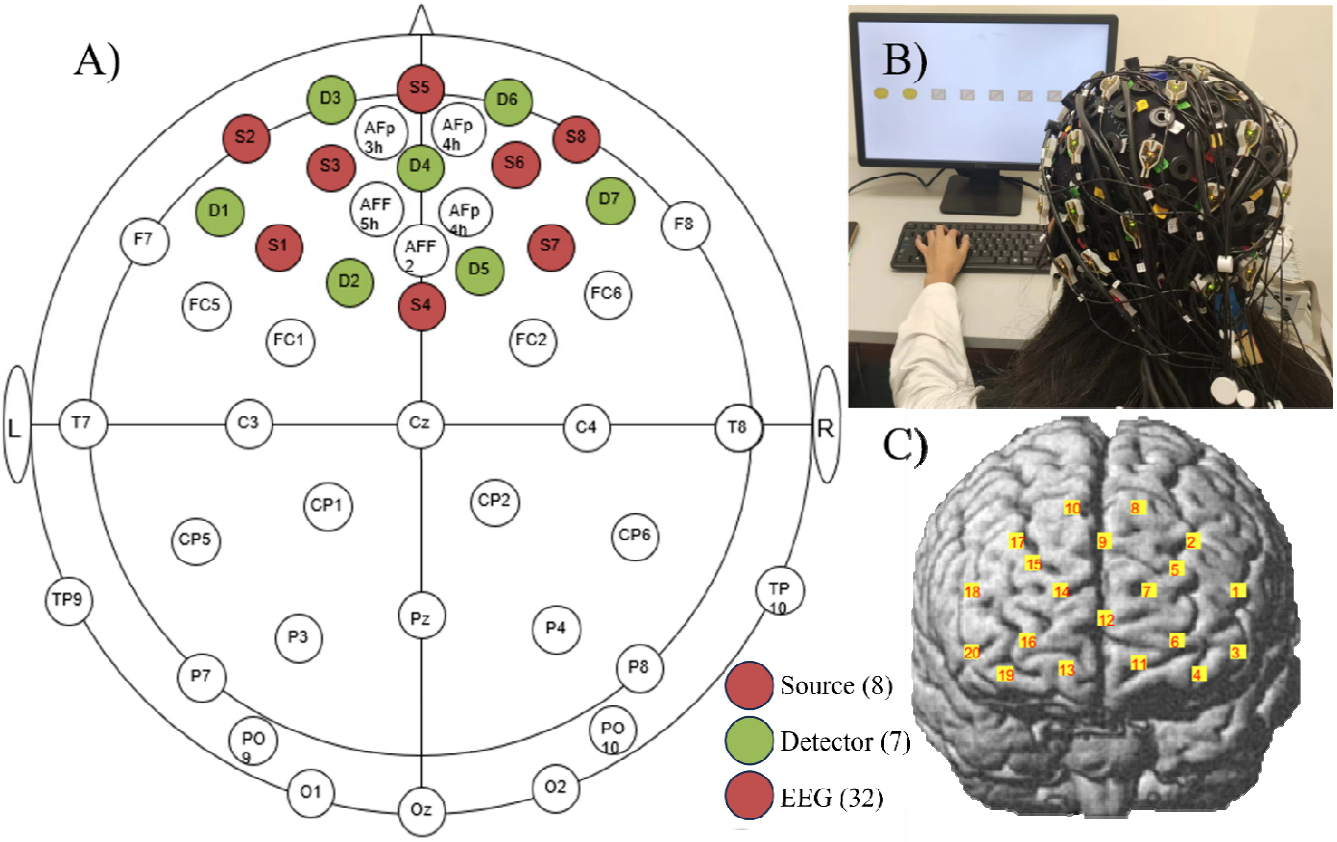

Fig. 2. The fNIRS-EEG device and location. A) The fNIRS channel and EEG location; B) The fNIRS-EEG device setup; C) fNIRS channels reconstructed by NIRS-SPM.

Table 1, 3D MNI coordinates, anatomical labels, and coverage percentage of fNIRS channels.

Channel Numbers	MNI	Anatomical label	Percentage of Overlap

	X	Y	Z		
1	-58.40	52.67	23.70	45 - pars triangularis Broca's area; 46 - Dorsolateral prefrontal cortex;	0.70556 0.29434
2	-40.65	58.09	47.26	9 - Dorsolateral prefrontal cortex; 46 - Dorsolateral prefrontal cortex;	0.47964 0.52036
3	-59.74	59.19	-4.02	10 - Frontopolar area; 45 - pars triangularis Broca's area; 46 - Dorsolateral prefrontal cortex; 47 - Inferior prefrontal gyrus;	0.0074074 0.018519 0.95556 0.018519
4	-41.86	76.99	-16.24	10 - Frontopolar area; 11 - Orbitofrontal area; 46 - Dorsolateral prefrontal cortex; 47 - Inferior prefrontal gyrus;	0.25385 0.42692 0.088462 0.23077
5	-32.54	69.63	36.72	9 - Dorsolateral prefrontal cortex; 10 - Frontopolar area; 46 - Dorsolateral prefrontal cortex;	0.0875 0.23333 0.67917
6	-32.42	82.00	0.95	10 - Frontopolar area; 11 - Orbitofrontal area;	0.52333 0.47667
7	-17.82	81.10	23.89	10 - Frontopolar area;	1
8	-14.86	61.44	64.43	8 - Includes Frontal eye fields; 9 - Dorsolateral prefrontal cortex;	0.020661 0.97934
9	-0.14	72.91	48.60	9 - Dorsolateral prefrontal cortex; 10 - Frontopolar area;	0.71654 0.28346
10	14.30	61.60	61.49	8 - Includes frontal eye fields; 9 - Dorsolateral prefrontal cortex;	0.020921 0.97908
11	-14.52	87.21	-11.00	10 - Frontopolar area; 11 - Orbitofrontal area;	0.29505 0.70395
12	0.07	86.32	11.93	10 - Frontopolar area;	1
13	14.68	87.20	-10.81	10 - Frontopolar area; 11 - Orbitofrontal area;	0.21429 0.78571
14	17.62	81.18	24.04	10 - Frontopolar area;	1
15	32.06	69.85	36.94	9 - Dorsolateral prefrontal cortex; 10 - Frontopolar area; 46 - Dorsolateral prefrontal cortex;	0.22041 0.31837 0.46122
16	32.23	82.06	1.31	10 - Frontopolar area; 11 - Orbitofrontal area;	0.47697 0.52303
17	40.01	58.56	47.48	9 - Dorsolateral prefrontal cortex; 46 - Dorsolateral prefrontal cortex;	0.63761 0.36239
18	57.77	53.36	24.15	45 - pars triangularis Broca s area; 46 - Dorsolateral prefrontal cortex;	0.57087 0.42913
19	41.60	77.12	-16.69	10 - Frontopolar area; 11 - Orbitofrontal area; 46 - Dorsolateral prefrontal cortex; 47 - Inferior prefrontal gyrus;	0.14449 0.55554 0.053232 0.23574
20	59.20	59.73	-3.39	10 - Frontopolar area; 46 - Dorsolateral prefrontal cortex; 47 - Inferior prefrontal gyrus;	0.051852 0.91481 0.033333

2.5 EEG data processing

2.5.1 Data Pre-processing

The EEG data were preprocessed using Matlab R2016a (MathWorks, Natick, USA) and EEGLAB, with a re-reference to grand average and a bandpass filter of 1-30 Hz. Independent Component Analysis (ICA) was applied to correct artifacts resulting from eye movements (blinks and shifts), muscle activity, and cardiac interference. Channels with high impedance were interpolated using the spherical method. Subsequently, the clean EEG data were segmented from 100 ms before the onset of the outcome to 1000 ms after the onset. Baseline correction was applied to all epochs, using the mean voltage over the 100 ms preceding the outcome onset as the reference. Epochs with EEG voltages exceeding a threshold of ±75 μV were excluded from further analysis. Two participants from HC group were excluded due to poor EEG signal quality, whose excluded epochs exceeded 20%.

2.5.2 Global field power analysis and ERP analysis

The global field power (GFP) was computed to assess the strength of the electric field at the scalp. GFP represents the square root of the average of the squared voltage values recorded at each electrode, serving as an index for the spatial standard deviation of the electric field at the scalp (Murray, Brunet, & Michel, 2008). A larger GFP value indicates a stronger electric field. Differences in GFP waveform data were analyzed in relation to time, specifically when the post-stimulus data significantly deviated from the baseline across conditions. The significance of GFP amplitude was determined by its consecutive exceedance of a 95% confidence interval for at least 20 ms relative to the 100-ms pre-stimulus baseline (Hua, Gao, Leong, & Yuan, 2023). Subsequently, GFP peaks were identified based on the averaged GFP waveform across all participants.

To identify topographic modulations, global map dissimilarity (GMD) measures were employed using randomization statistics. GMD is calculated as the root mean square of the difference between strength-

normalized vectors (Murray, Brunet et al., 2008). Differences in GMD values were also analyzed with respect to time. The statistical significance of GMD was determined using a topographic analysis of variance (ANOVA) with 10,000 permutations ($p < 0.05$). GMD results indicate differences in neural generators across conditions, which are independent of field strength. The significance levels of GMD results were adjusted using a duration threshold of 20 ms.

In the present study, electrodes located in the central regions were selected for analysis: FC1, FC2, C3, C4, CP1, CP2 by GFP findings. all the trials for each participant were averaged and conducting paired two-sided t-tests and independent two-sided t-tests to test for significant differences in relation to feedback outcomes and group. The *p* values were corrected using the false discovery rate (FDR) with a significance level of $p = 0.05$.

2.5.3 Time-frequency analysis

Event-related oscillations (EROs) were computed using MNE Python software 1.2 to explore the potential brain oscillations associated with ERPs. Morlet wavelets were used to extract the time-frequency representation of induced power at each time point (550 data points, ranging from -100 ms to 1000 ms relative to feedback onset) and frequency (4-30 Hz with a resolution of 2 Hz) (Morales & Bowers, 2022). The Morlet wavelet transform is commonly employed for calculating EEG spectral components, as it strikes a favorable balance between temporal and frequency resolution. Moreover, it demonstrates exceptional efficiency when applied to non-stationary signals, making it suitable for this study (Vecchio, Nucci, Pappalettera, Miraglia, Iacoviello, & Rossini, 2022). Statistical analysis of EROs was performed using a non-parametric procedure based on permutations (1000 times) and cluster-level statistics ($p = 0.001$, cluster-level $p = 0.01$).

2.5.4 Multivariate pattern analysis

MVPA was employed to examine the topographic weighting of EEG signals that effectively differentiated between win and loss feedback within specific time intervals, utilizing MNE Python software version 1.2. A linear classifier based on L2-regularized logistic regression was used to identify optimal projections of the sensor space, enabling discrimination between win and loss feedback in individuals with IGDs and HCs at specific time points. This approach allowed for the investigation of feedback perception availability in IGDs and HCs based on stimulus-locked EEG data, and the temporal dynamics of this availability were evaluated using time-resolved decoding.

The accuracy of the linear L2-regularized logistic regression classifier, trained on multi-electrode single-trial EEG signals, was independently assessed for each time point. A Monte Carlo cross-validation procedure (n = 100) was employed, repeated for 10 times, with the entire dataset randomly partitioned into 10 subsets consisting of a training set (90% of the trials) and a test set (the remaining 10%). These time windows corresponded to the ERP and ERO analyses, spanning from 100 ms before the stimulus onset to 1000 ms after the stimulus onset. Individual classification accuracy was considered statistically above chance when it exceeded the classification accuracy obtained from permuted labels (paired t-test, $\alpha = 0.05$). Group-level analysis followed the same procedure, with group averages computed across individual subject averages. Correction for multiple comparisons was achieved using a time-cluster-based approach, where a time point was considered significant only if it belonged to a cluster comprising at least twenty consecutive significant time points.

2.6 fNIRS data analysis

fNIRS signals from five participants (three in IGD group and two in HCs) were not recorded due to machine malfunction, and one HC was excluded due to low-quality signals. The fNIRS data were

preprocessed using the nirsLAB toolbox (NIRx Medizintechnik GmbH, Berlin, Germany). Motion artifacts were removed and detrending was applied to the raw data using the built-in algorithm. To achieve the best signal-to-noise ratio, the data were further band-pass filtered with a low cutoff frequency of 0.1 Hz and a high cutoff frequency of 0.01 Hz to minimize physiological noise associated with heart pulsation (1-1.5 Hz), respiration (0.2-0.5 Hz), and blood pressure waves (~0.1 Hz) (Lu, Wang, Xu, Chen, Yuan, Luo et al., 2021). The HbO changes were modeled using statistical parametric mapping with the canonical hemodynamic response function. This resulted in general linear model coefficients (beta values) across all conditions for each participant. In this study, only HbO signals were analyzed as they provide a more sensitive indicator of changes associated with regional cerebral blood flow (Xu, Lu, Wang, Hu, Zhang, Chen et al., 2020). Subsequently, the beta values of feedback perception in each channel were compared using a two-way ANOVA and corrected using FDR.

Following a case-control study protocol, the statistical analyses were conducted using R software 3.6 and MATLAB 2016. Risk-taking behavior was defined as the number of opened win boxes in the gain condition, which reflects a standard measure in sequential risk-taking tasks (Z. Liu, Cheng et al., 2020). Two-way ANOVA analysis was used to explore the factors (participants and outcome of the last trial) that affected risk behaviors in the subsequent trial. Continuous demographic data (age, DSM-V, CIAS, BIS-11) were compared using independent t-tests, and gender distribution between the two groups was compared using a chi-squared test. The statistics for EEG and fNIRS analyses are described in each respective section. The parameters of computational models were compared using independent t-tests. Potential correlations between demographic data (CIAS, BIS-11) and modeling parameters, as well as the number of boxes opened in the gain condition, were explored using Pearson correlation.

3 Results

3.1 Demographic data

There were no significant differences in age and gender between the IGDs and HCs (Table 2). However, significant differences were observed in education levels, DSM-V scores, CIAS score, and BIS-11 scores between the IGD and HC groups.

Table 2: Demographic and personality characteristics of the included participants.

	IGD (15) **Mean (std)**	**HC (27)** **Mean (std)**	***t* value**	***p* value**
Age	21.4667 (1.993)	21.667 (2.019)	-0.3252	0.7472
Gender	6 female / 9 male	17 female /10 male	X^2=1.23	0.2674
Education	14.4667 (1.1254)	15.481 (1.889)	-2.181	0.0352
DSM-V	6.6 (0.8281)	1.926 (0.8738)	17.183	<0.001
BIS-11	61.533 (5.0124)	47.481 (5.366)	8.4867	<0.001
CIAS	77.20 (7.013)	40.037 (6.531)	16.861	<0.001

3.2 Behavioral analysis

The results revealed that individuals with IGD exhibited a higher propensity to open more boxes compared to the HC group (F (2, 40) = 12.397, p = 0.0007, Fig 3 Panel A). Interestingly, both the IGD and HC groups showed a greater likelihood of opening boxes after negative outcomes compared to positive outcomes, as indicated by paired t-tests (IGD: boxes opened $_{Gain}$ = 3.914 ± 0.763, boxes opened $_{Lose}$ = 4.111 ± 0.737, t = -2.550, p = 0.03; HC: boxes opened $_{Gain}$ = 3.402 ± 0.574, boxes opened $_{Lose}$ = 3.620 ± 0.519, t = -3.135, p = 0.004).

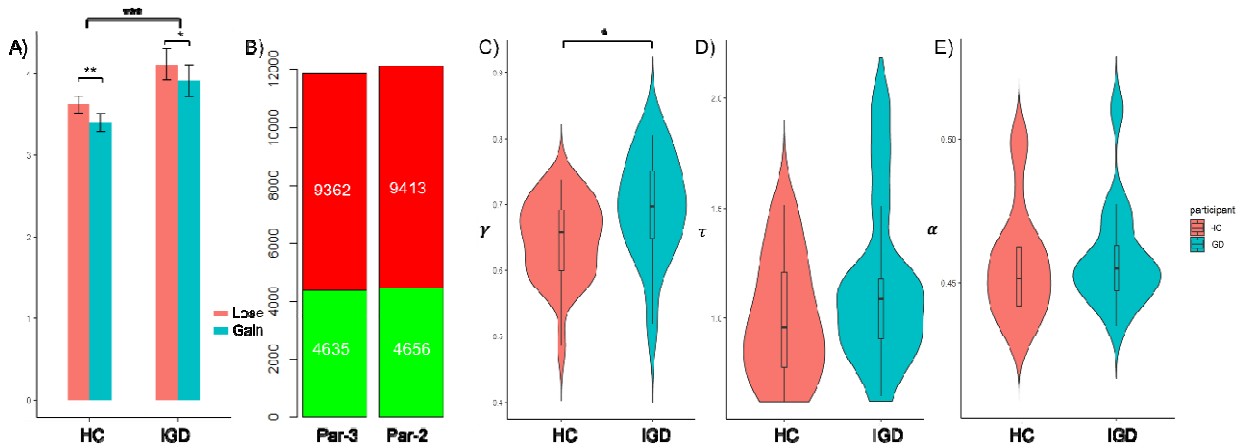

Fig. 3. The behavioral and modeling results. A) The opened boxes in gain condition after lose condition and win condition in both HCs and IGDs; B) The LOOIC values of the two models; C) The computational modeling parameter rho, indicating risk-taking propensity; D) The computational modeling parameter tau, indicating inverse temperature; E) The computational modeling parameter alpha, indicating emotional affection. *** indicates $p < 0.001$; ** indicates $p < 0.01$; * indicates $p < 0.05$.

3.3 Modeling results

The results of model comparison using the leave-one-out information criterion (LOOIC) indicated that the Par-3 model, which considered the impact of emotional influence, provided a better fit to the data compared to the Par-2 model (Fig 3 Panel B).

The posterior distributions of the fitted Par-3 model parameters were calculated to quantify the underlying cognitive processes during the sequential risk-taking task. The IGD group exhibited a significantly higher risk-taking propensity ($\lambda_{IGD} = 0.697 \pm 0.058$) compared to the HC group ($\lambda_{HC} = 0.644 \pm 0.077$, $t = 2.339$, $p = 0.0284$, Fig 3 Panel C). However, no significant differences were found between the two groups in terms of behavioral consistency ($\tau_{IGD} = 1.295$, $\tau_{HC} = 1.165$, $t = 0.374$, $p = 0.7117$, Fig 3 Panel D) or emotional affection ($a_{IGD} = 0.484$, $a_{HC} = 0.481$, $t = 0.631$, $p = 0.533$, Fig 3 Panel E).

3.4 GFP and ERP results

Both the IGD and HC groups exhibited significantly different neural responses to negative and positive feedbacks from 50 ms to 460 ms. Three time windows of GFP peaks at 50-86 ms, 114-164 ms, and 280-460 ms were identified as significantly different between the four conditions, corresponding to P1, feedback-related negativity (FRN), and P3, respectively. In the HC and IGD groups, positive feedbacks resulted in higher electric field strength in the 50-86 ms time window (higher positive potential in the

central region and higher negative potential in the occipital region), as well as lower electric field strength in the 280-460 ms time window (lower positive potential in the central region), compared to negative feedbacks. Additionally, compared to the HC group, the negative feedbacks in the IGD group induced significant differences in electric field strength (lower positive potential in the prefrontal region and lower negative potential in the occipital region) in the 114-164 ms time window. No significant differences in the topographical distribution of the electric field, independent of the electric field strength, were found after positive feedbacks between the IGD and HC groups.

Interestingly, in both the IGD and HC groups, negative feedbacks elicited a higher P1 amplitude, lower FRN amplitude, and higher P300 amplitude compared to positive feedbacks. Furthermore, a significant difference in ERP components was observed, with the IGD group showing a shorter P300 latency

compared to the HC group.

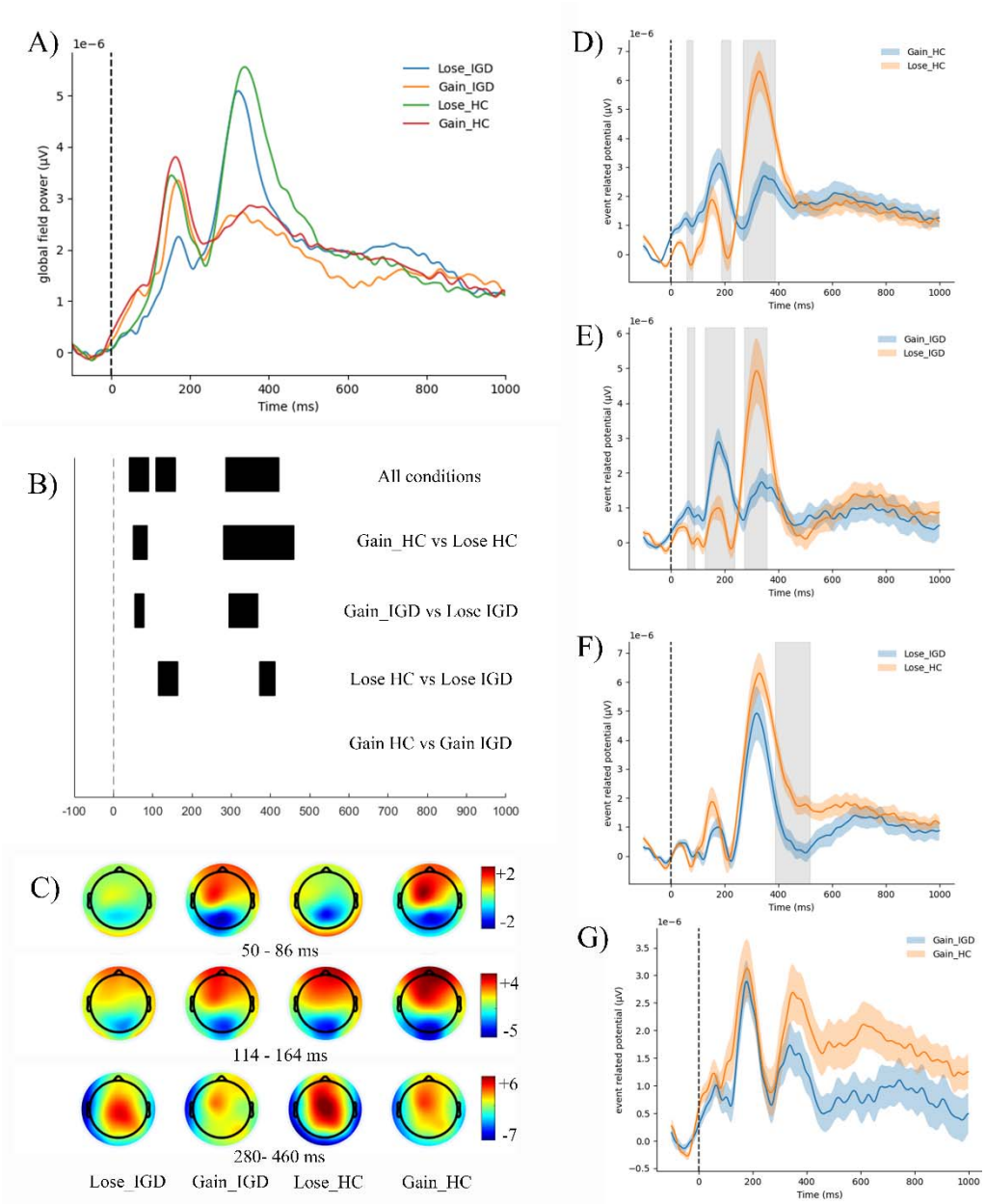

Fig. 4. Neural responses to feedbacks exhibited difference in GFP and ERP. **A).** The GFP to lose/gain feedbacks in both IGD and HC; **B).** The time segments of significant GMD were indicated in black bars. The top row depicted the significant main difference of the four conditions, while the rest rows depicted pairwise comparisons (HC_{Gain} vs HC_{Lose}, IGD_{Gain} vs IGD_{Lose}, HC_{Gain} vs IGD_{Gain}, HC_{Lose} vs IGD_{Lose}); **C).** Topography among the four conditions in three time windows (50-86 ms, 114-164 ms, and 280-460 ms). For each topography, EEG signals were averaged

across time points within a specific time window. Color bar denotes the voltage value (μV).; **D-F).** The ERP pairwise comparison to lose/gain feedbacks in both IGDs and HC; colored shaded area: mean±error bar; light gray shaded area: the period of significant decoding at the group level ($p_{FDR} < 0.05$).

3.5 ERO results

Significant differences in frequency spectra between positive and negative feedbacks were observed in both the IGD and HC groups. In the HC group, delta power of EROs after negative feedbacks was significantly higher in the 174-532 ms time window compared to positive feedbacks. Similarly, in the IGD group, higher delta power of EROs was found in the 192-456 ms time window. No significant differences in frequency spectra after positive or negative feedbacks were found in either the IGD or HC group.

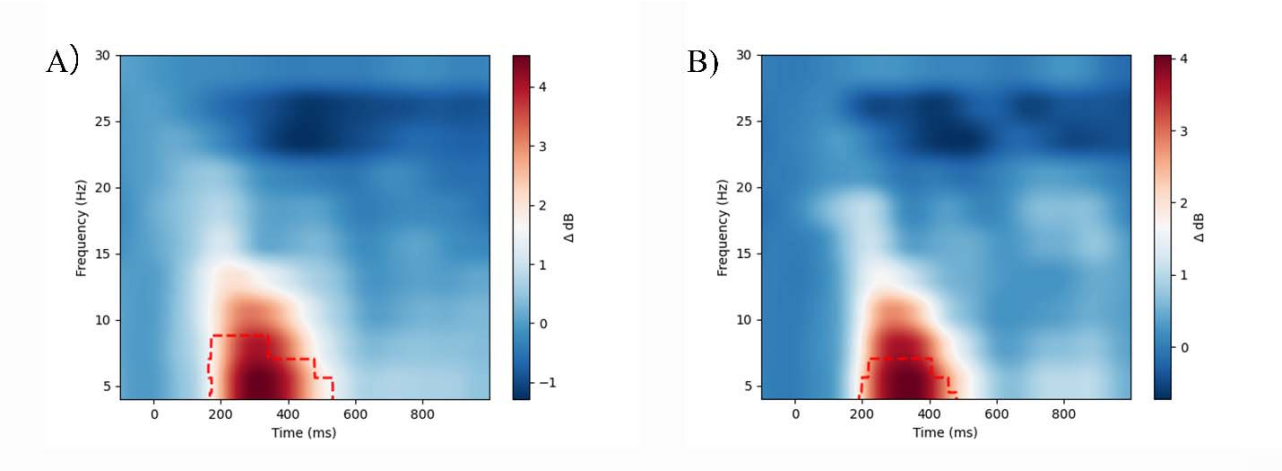

Fig. 5. EROs to feedbacks exhibited difference. A) EROs to lose feedback, contrasting to gain feedback of EROs in HCs; B) EROs to lose feedback, contrasting to gain feedback of EROs in IGDs.

3.6 One-vs-one decoding results

To further examine how the global perceived orientation varied across the four conditions, one-vs-one classification was performed for all paired comparisons. Pairwise classifications yielded significant accuracies above chance level at specific time points across the trials ($p < 0.05$, lasting for > 20 ms). In the HC group, pronounced decoding performance was observed between positive and negative feedbacks, roughly from 140 to 570 ms, indicating a long-lasting neural response difference. In the IGD group, the decoding performance between positive and negative feedbacks ranged from 190 to 380 ms. Notably, the time window between 330 to 520 ms showed a highly significant discrimination effect between IGD and HC using the neural response to negative feedback. Additionally, a short-lived group difference between IGD and HC was observed after perceiving positive feedbacks in the time window 330-380 ms.

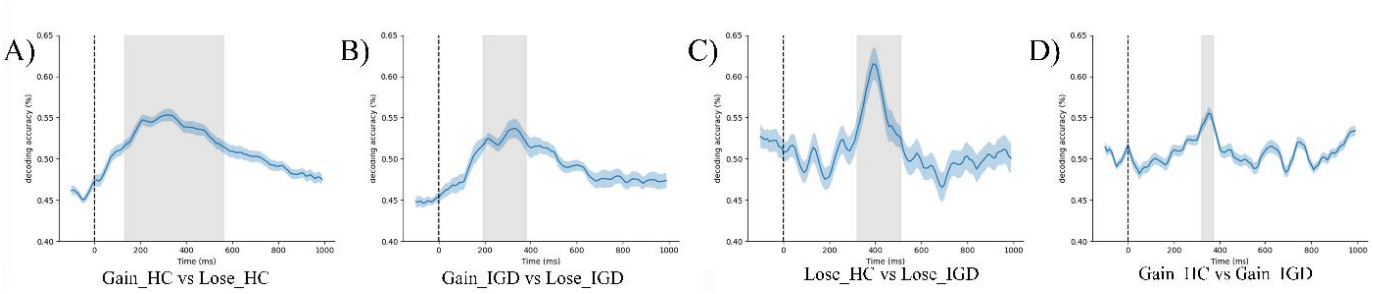

Fig. 6. One-vs-one decoding results across time. A-D). Pairwise decoding between the four conditions. Colored curves indicate decoding accuracy averaged across participants. Colored shaded area: bootstrapped 95% confidence interval; light gray shaded area: the period of significant decoding at the group level ($p < 0.05$ lasting for > 20 ms).

3.7 fNIRS results

To verify if the abnormal corresponding neural response to feedbacks also occurred in the IGD group compared to HCs, brain activation regions in the PFC were identified using fNIRS neuroimaging. Pairwise t-tests demonstrated significantly lower activation after positive feedbacks in the IGD group compared to the HC group in channel 4 ($t = -3.003$, $p = 0.0051$, covering 36.09% frontopolar area, 42.692% orbitofrontal area, 23.087% inferior prefrontal gyrus), channel 11 ($t = -2.94$, $p = 0.0063$, covering 29.605%

frontopolar area, 70.395% orbitofrontal area), and channel 13 (t = -2.89, p = 0.0072, covering 21.429% frontopolar area, 78.571% orbitofrontal area). Similarly, significantly lower activation after negative feedbacks was observed in the IGD group compared to the HC group in channel 7 (t = -3.22, p = 0.0031, covering 100% frontopolar area) and channel 14 (t = -3.19, p = 0.0033, covering 100% frontopolar area).

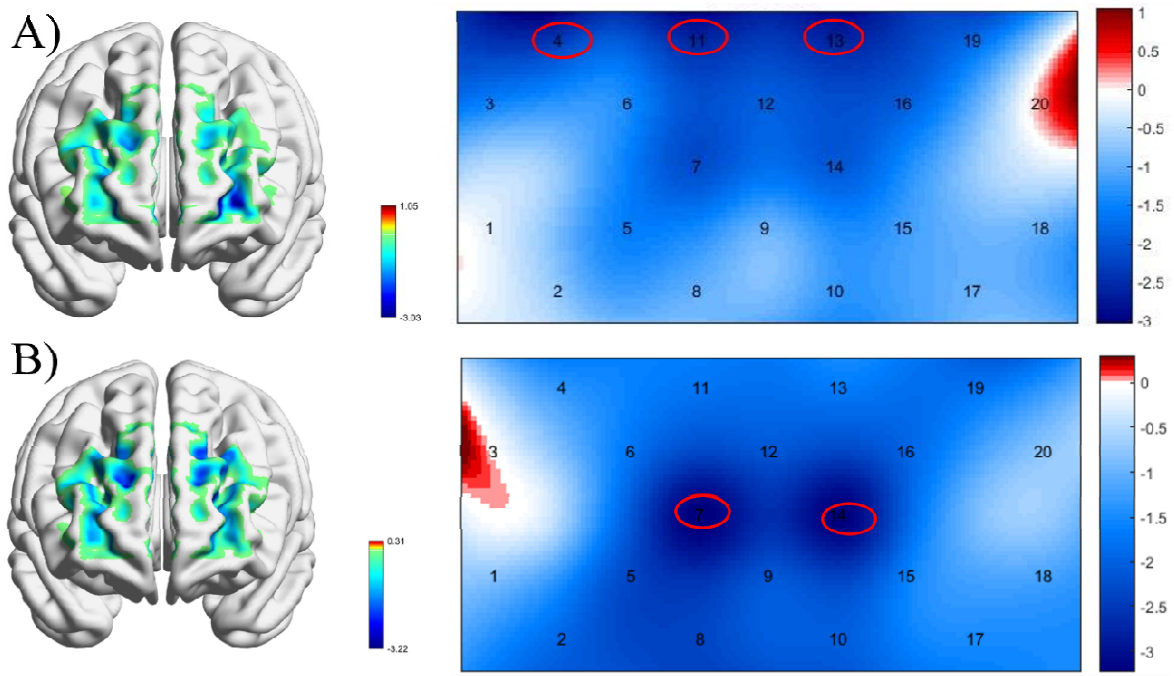

Fig. 7. fNIRS activation contrast between IGDs and HCs. A). The activation difference after positive feedbacks in IGDs compared to HCs; B) The activation difference after negative feedbacks in IGDs compared to HCs; The color bar indicated the t value of contrast.

3.8 Correlation results

Our correlation results found that the risk propensity ( ) was positively correlated with BIS-11 scores in both HCs (r =0.47, p = 0.013) and IGDs (r =0.61, p = 0.016), while BIS-11 was also positively correlated with boxes opened in IGD (r =0.54, p = 0.036) (Figure 8). No other correlational relations were found.

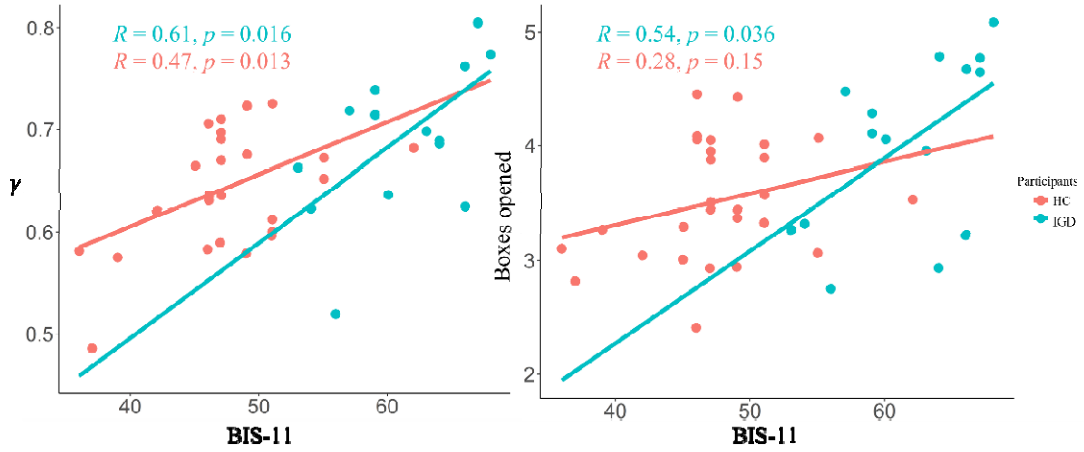

Fig. 8. The correlations between demographic data and behavioral data, modelling data in both IGDs and HCs.

Discussion

Through the implementation of a sequential risk-taking task and computational modeling, our study revealed that individuals with IGD exhibited a higher propensity for engaging in risky decision-making compared to HCs. Neuroimaging data, including neurophysiological responses P300 and fNIRS assessment of PFC activation, demonstrated distinct neural responses of perceiving outcomes among individuals with IGD compared to HCs. Additionally, our findings have highlighted the impact of outcome valence on subsequent decision-making performance via behavioral results and neuroimaging findings Interestingly, negative outcomes tend to exert a stronger influence on risk-taking propensity compared to positive outcomes. Leveraging the power of neuroimaging techniques, we have identified noteworthy variations in neural responses during the P100 and P300 time windows following feedback processing. Furthermore, alterations of theta power brain oscillations in both IGDs and HCs have been observed, particularly in relation to negative outcomes, compared to positive outcomes.

First, our behavioral results and modeling parameter findings indicate that individuals with IGD exhibit a heightened inclination towards risk-taking behaviors compared to HCs, which is consistent with previous

research on risky propensity of IGD in both ambiguity decision making (Jiang, Li, Zhou, & Zhou, 2020; J. Kim & Kang, 2018) and risky decision making (Ko, Wang et al., 2017; Q. Li, Wang et al., 2020; L. Liu, Xue et al., 2017). The increased risk propensity observed in individuals with IGD can be attributed to dysregulated reward processing, imbalanced cost-benefit weighting, and poor impulse control. Reward processing refers to the way the brain evaluates and responds to rewarding stimuli, such as pleasurable experiences or outcomes (Meyer, Marco-Pallarés, Boulinguez, & Sescousse, 2021). Previous studies have characterized IGD as an impairment in the reward circuit, with individuals excessively pursuing rewards (L. Wang, Yang, Zheng, Li, Qi, Li et al., 2021). This heightened response to rewards can lead individuals with IGD to be more willing to take risks in pursuit of immediate rewards, often disregarding potential negative consequences or losses (Weinstein & Lejoyeux, 2020). Delay discounting tasks have shown that individuals with IGD are more likely to prioritize immediate rewards (Weinsztok, Brassard, Balodis, Martin, & Amlung, 2021). Additionally, imbalanced cost-benefit weighting, where the expected effect of risky behaviors outweighs the potential negative consequences, contributes to a higher propensity for harmful risk-taking behaviors in individuals with IGD (Hong, Liang, Pan, Jin, Luo, Li et al., 2023). While individuals with IGD and HCs may demonstrate similar risk propensities when risky behaviors are favorable, individuals with IGD exhibit significantly higher risk propensities when faced with unfavorable outcomes (Y. W. Yao, Chen et al., 2015). Lastly, in addition to dysregulated reward processing and imbalanced cost-benefit weighting, poor impulse control might be associated with risky decision making among IGDs. inhibition control plays a crucial role in decision-making to maximize advantages (Sakagami, Pan, & Uttl, 2006). Consequently, previous studies have found that impaired inhibitory control predicted higher addiction degrees and more impulsive in decision making among IGDs (Kräplin, Scherbaum, Kraft, Rehbein, Bühringer, Goschke et al., 2020; Y. W. Yao, Wang, Yip, Chen, Li, Xu et al., 2015). The impaired response inhibition and salience attribution (iRISA) model suggests that deficits in inhibition control are core impairments in addiction (Zilverstand, Huang, Alia-Klein, & Goldstein, 2018). Our findings are consistent to this model, as our correlational findings revealed a

significantly positive correlation between impulsivity (BIS-11 scores) and risk-taking propensity. As such, impaired inhibition control may be associated with riskier behaviors in sequential risk-taking tasks.

In addition, our study demonstrated significantly different neural responses to feedback among individuals with IGD compared to HCs, as measured by the combined EEG-fNIRS fusion technique. We consistently observed a significant neural response in the P300 time window (300-500 ms) towards negative outcomes in both IGD and HCs using GMD, ERP, and MVPA. The P300 component is a positive-going waveform recorded at centro-parietal sites occurring approximately 300-600 ms after stimulus onset (Yu, Liu, & Shi, 2020), which has been found been associated with processing capacity, mental workload, and also thought to be related to cost-benefit evaluation and decision-making computations (Gui, Li, Li, & Luo, 2016; Kok, 2001). The lower GMD and shorter P300 latency suggested that individuals with IGD made more intuitive decisions in response to feedback. Previous ERP studies have shown that individuals with IGD exhibited reduced P300 amplitudes during auditory information processing, compared to HCs (M. Park, Kim, & Choi, 2016). Also, Y. Zhou, Yao, Fang, and Gao (2022) investigated P300 effects in decision-making processes among individuals with IGD and recreational gaming users but did not find differences between the two groups. There are two possible explanations for this discrepancy. Firstly, our study compared neural responses between individuals with IGD and non-gaming users. Recreational gaming users share more similarity with IGDs in behaviors and brain compared to non-gaming users (Infanti, Valls-Serrano, Perales, Vögele, & Billieux, 2023). Secondly, our study specifically examined neural responses following negative feedback, not the neural response during decision making.

Consistent with previous research, we found reduced activation in the PFC among individuals with IGD after feedback perception, a region known to play important roles in decision-making (St. Onge & Floresco, 2009). Adopting risky decision-making paradigms and neuroimaging tools, Dong and Potenza (2016) observed lower activations in the inferior frontal gyrus while L. Liu, Xue et al. (2017) found

increased responses in the ventral striatum among individuals with IGD when presented with rewarding outcomes. Higher activation in the reward system may impair the executive control system (Goldstein & Volkow, 2011). Thus, the heightened neural response to feedback among individuals with IGD suggested an enhanced sensitivity to rewards and punishments, indicating dysregulation in the neural circuits involved in reinforcement learning and decision-making processes (Zhang, Hu, Wang, Wang, & Dong, 2020).

Our study found that negative outcomes in decision-making have a significant impact on subsequent decision-making behaviors and elicit distinct neural responses, compared to positive outcomes. The influence of feedback on decision-making patterns can be categorized into two distinct patterns: "cold" cognitive patterns and "hot" emotional responses (Y. Zhou, Yao et al., 2022). The "cold" cognitive patterns are associated with the central executive network, which evaluates and optimizes decision-making strategies to maximize profit (Salehinejad, Ghanavati, Rashid, & Nitsche, 2021). On the other hand, the feedbacks also trigger emotional and involuntary responses in the body, such as increased heart rate, visceral reactions, perspiration, relief, and regret emotions, which are mediated by the affective network (Weinstein & Lejoyeux, 2020). Our modeling data showed that considering the emotional rating from the previous trial improved the performance of the models, demonstrating that behaviors can be influenced by emotional responses. Negative outcomes tend to elicit stronger emotional responses, which may restrict the involvement of the central executive network (Hsu, Bhatt, Adolphs, Tranel, & Camerer, 2005; Tom, Fox, Trepel, & Poldrack, 2007). Additionally, we observed higher theta oscillations between positive and negative feedbacks. This finding is consistent with previous studies indicating that theta oscillations are feedback-related signals and are commonly elicited by incorrect outcomes in these tasks (Y. Wang, Cheung, Yee, & Tse, 2020).

While our study sheds light on the relationship between risky decision-making, neural responses to feedback, and IGD, several limitations should be considered. Firstly, the sample size in our study was

relatively small, which may limit the generalizability of the findings. Future research with larger and more diverse samples is necessary to validate and further explore these findings. Additionally, although we excluded patients diagnosed with psychiatric disorders such as anxiety and depression, we did not specifically measure the degree of anxiety and depression among the included participants. This could be taken into consideration in future investigations.

Conclusion

In summary, our study uncovered that individuals with IGDs exhibit a significant propensity for risk-taking behaviors compared to HCs. This inclination is linked to dysregulated reward processing, poor impulse control, and inhibited inhibitory mechanisms. Neuroimaging results support these findings, showing a heightened sensitivity to rewards and a dearth of cognitive control in IGD. Our insights provide a foundation for future research and potential interventions in the domain of risky decision-making among individuals with IGD.

Reference

Ahn, W. Y., Haines, N., & Zhang, L. (2017). Revealing Neurocomputational Mechanisms of Reinforcement Learning and Decision-Making With the hBayesDM Package. *Comput Psychiatr, 1*, 24-57. doi:10.1162/CPSY_a_00002

Argyriou, E., Davison, C. B., & Lee, T. T. C. (2017). Response Inhibition and Internet Gaming Disorder: A Meta-analysis. *Addict Behav, 71*, 54-60. doi:10.1016/j.addbeh.2017.02.026

Brassen, S., Gamer, M., Peters, J., Gluth, S., & Büchel, C. (2012). Don't look back in anger! Responsiveness to missed chances in successful and nonsuccessful aging. *Science, 336*(6081), 612-614. doi:10.1126/science.1217516

Chen, S.-H., Weng, L.-J., Su, Y.-J., Wu, H.-M., & Yang, P.-F. J. C. J. o. P. (2003). Development of a Chinese Internet addiction scale and its psychometric study.

Deleuze, J., Nuyens, F., Rochat, L., Rothen, S., Maurage, P., & Billieux, J. (2017). Established risk factors for addiction fail to discriminate between healthy gamers and gamers endorsing DSM-5 Internet gaming disorder. *J Behav Addict, 6*(4), 516-524. doi:10.1556/2006.6.2017.074

Derevensky, J. L., Hayman, V., & Lynette, G. (2019). Behavioral Addictions: Excessive Gambling, Gaming, Internet, and Smartphone Use Among Children and Adolescents. *Pediatr Clin North Am, 66*(6), 1163-1182. doi:10.1016/j.pcl.2019.08.008

Dong, G., & Potenza, M. N. (2016). Risk-taking and risky decision-making in Internet gaming disorder: Implications regarding online gaming in the setting of negative consequences. *J Psychiatr Res, 73*, 1-8. doi:10.1016/j.jpsychires.2015.11.011

Figner, B., Mackinlay, R. J., Wilkening, F., & Weber, E. U. (2009). Affective and deliberative processes in risky choice: age differences in risk taking in the Columbia Card Task. *J Exp Psychol Learn Mem Cogn, 35*(3), 709-730. doi:10.1037/a0014983

Gao, F., Hua, L., He, Y., Xu, J., Li, D., Zhang, J., & Yuan, Z. (2023). Word structure tunes electrophysiological and hemodynamic responses in the frontal cortex. *Bioengineering, 10*(3), 288.

Gao, F., Wang, R., Armada-da-Silva, P., Wang, M.-Y., Lu, H., Leong, C., & Yuan, Z. (2022). How the brain encodes morphological constraints during Chinese word reading: An EEG-fNIRS study. *Cortex, 154*, 184-196.

Goldstein, R. Z., & Volkow, N. D. (2011). Dysfunction of the prefrontal cortex in addiction: neuroimaging findings and clinical implications. *Nature Reviews Neuroscience, 12*(11), 652-669. doi:10.1038/nrn3119

Grootswagers, T., Wardle, S. G., & Carlson, T. A. (2017). Decoding Dynamic Brain Patterns from Evoked Responses: A Tutorial on Multivariate Pattern Analysis Applied to Time Series Neuroimaging Data. *J Cogn Neurosci, 29*(4), 677-697. doi:10.1162/jocn_a_01068

Gui, D.-Y., Li, J.-Z., Li, X., & Luo, Y.-j. (2016). Temporal Dynamics of the Interaction between Reward and Time Delay during Intertemporal Choice. *7*. doi:10.3389/fpsyg.2016.01526

Hong, W., Liang, P., Pan, Y., Jin, J., Luo, L., Li, Y., . . . Zhang, X. (2023). Reduced loss aversion in value-based decision-making and edge-centric functional connectivity in patients with internet gaming disorder. *J Behav Addict, 12*(2), 458-470. doi:10.1556/2006.2023.00014

Hsu, M., Bhatt, M., Adolphs, R., Tranel, D., & Camerer, C. F. (2005). Neural systems responding to degrees of uncertainty in human decision-making. *Science, 310*(5754), 1680-1683. doi:10.1126/science.1115327

Hua, L., Gao, F., Leong, C., & Yuan, Z. (2023). Neural decoding dissociates perceptual grouping between proximity and similarity in visual perception. *Cereb Cortex, 33*(7), 3803-3815. doi:10.1093/cercor/bhac308

Infanti, A., Valls-Serrano, C., Perales, J. C., Vögele, C., & Billieux, J. (2023). Gaming passion contributes to the definition and identification of problematic gaming. *Addict Behav, 147*, 107805. doi:10.1016/j.addbeh.2023.107805

Jiang, C., Li, C., Zhou, H., & Zhou, Z. (2020). Individuals with internet gaming disorder have similar neurocognitive impairments and social cognitive dysfunctions as methamphetamine-dependent patients. *Adicciones, 0*(0), 1342. doi:10.20882/adicciones.1342

Kim, J., & Kang, E. (2018). Internet Game Overuse Is Associated With an Alteration of Fronto-Striatal Functional Connectivity During Reward Feedback Processing. *Front Psychiatry, 9*, 371. doi:10.3389/fpsyt.2018.00371

Kim, Y. J., Lee, J.-Y., Oh, S., Park, M., Jung, H. Y., Sohn, B. K., . . . Choi, J.-S. (2017). Associations between prospective symptom changes and slow-wave activity in patients with Internet gaming disorder: A resting-state EEG study. *96*(8), e6178. doi:10.1097/md.0000000000006178

Ko, C. H., Wang, P. W., Liu, T. L., Chen, C. S., Yen, C. F., & Yen, J. Y. (2017). The adaptive decision-making, risky decision, and decision-making style of Internet gaming disorder. *Eur Psychiatry, 44*, 189-197. doi:10.1016/j.eurpsy.2017.05.020

Ko, C. H., Yen, J. Y., Yen, C. F., Chen, C. S., & Chen, C. C. (2012). The association between Internet addiction and psychiatric disorder: a review of the literature. *Eur Psychiatry, 27*(1), 1-8. doi:10.1016/j.eurpsy.2010.04.011

Kok, A. (2001). On the utility of P3 amplitude as a measure of processing capacity. *Psychophysiology, 38*(3), 557-577. doi:10.1017/s0048577201990559

Kräplin, A., Scherbaum, S., Kraft, E. M., Rehbein, F., Bühringer, G., Goschke, T., & Mößle, T. (2020). The role of inhibitory control and decision-making in the course of Internet gaming disorder. *J Behav Addict, 9*(4), 990-1001. doi:10.1556/2006.2020.00076

Kusev, P., Purser, H., Heilman, R., Cooke, A. J., Van Schaik, P., Baranova, V., . . . Ayton, P. (2017). Understanding Risky Behavior: The Influence of Cognitive, Emotional and Hormonal Factors on Decision-Making under Risk. *Front Psychol, 8*, 102. doi:10.3389/fpsyg.2017.00102

Lee, M. D. (2011). How cognitive modeling can benefit from hierarchical Bayesian models. *Journal of Mathematical Psychology, 55*(1), 1-7. doi:https://doi.org/10.1016/j.jmp.2010.08.013

Li, Q., Wang, Y., Yang, Z., Dai, W., Zheng, Y., Sun, Y., & Liu, X. (2020). Dysfunctional cognitive control and reward processing in adolescents with Internet gaming disorder. *Psychophysiology, 57*(2), e13469. doi:10.1111/psyp.13469

Li, R., Yang, D., Fang, F., Hong, K. S., Reiss, A. L., & Zhang, Y. (2022). Concurrent fNIRS and EEG for Brain Function Investigation: A Systematic, Methodology-Focused Review. *Sensors (Basel), 22*(15). doi:10.3390/s22155865

Li, X.-y., Phillips, M. R., Xu, D., Zhang, Y.-l., Yang, S.-j., Tong, Y.-s., . . . Niu, Y.-J. J. C. M. H. J. (2011). Reliability and validity of an adapted Chinese version of Barratt Impulsiveness Scale.

Li, Y., Chen, R., Zhang, S., Turel, O., Bechara, A., Feng, T., . . . He, Q. (2019). Hemispheric mPFC asymmetry in decision making under ambiguity and risk: An fNIRS study. *Behav Brain Res, 359*, 657-663. doi:10.1016/j.bbr.2018.09.021

Liu, L., Xue, G., Potenza, M. N., Zhang, J. T., Yao, Y. W., Xia, C. C., . . . Fang, X. Y. (2017). Dissociable neural processes during risky decision-making in individuals with Internet-gaming disorder. *Neuroimage Clin, 14*, 741-749. doi:10.1016/j.nicl.2017.03.010

Liu, Z., Cheng, X., Liu, S., Zhang, Z., Li, S., Li, L., & Guo, X. (2020). Attentional deployment training impacts neural responses to subsequent regret. *International Journal of Psychophysiology, 157*, 23-31. doi:10.1016/j.ijpsycho.2020.08.002

Lu, F., Wang, M., Xu, S., Chen, H., Yuan, Z., Luo, L., . . . Zhou, J. (2021). Decreased interhemispheric resting-state functional connectivity in male adolescents with conduct disorder. *Brain Imaging Behav, 15*(3), 1201-1210. doi:10.1007/s11682-020-00320-8

Luo, T., Wei, D., Guo, J., Hu, M., Chao, X., Sun, Y., . . . Liao, Y. (2021). Diagnostic Contribution of the DSM-5 Criteria for Internet Gaming Disorder. *Front Psychiatry, 12*, 777397. doi:10.3389/fpsyt.2021.777397

Meyer, G. M., Marco-Pallarés, J., Boulinguez, P., & Sescousse, G. (2021). Electrophysiological underpinnings of reward processing: Are we exploiting the full potential of EEG? *Neuroimage, 242*, 118478. doi:10.1016/j.neuroimage.2021.118478

Morales, S., & Bowers, M. E. (2022). Time-frequency analysis methods and their application in developmental EEG data. *Dev Cogn Neurosci, 54*, 101067. doi:10.1016/j.dcn.2022.101067

Murray, M. M., Brunet, D., & Michel, C. M. (2008). Topographic ERP analyses: a step-by-step tutorial review. *Brain Topogr, 20*(4), 249-264. doi:10.1007/s10548-008-0054-5

Oskarsson, A. T., Van Boven, L., McClelland, G. H., & Hastie, R. (2009). What's next? Judging sequences of binary events. *Psychol Bull, 135*(2), 262-285. doi:10.1037/a0014821

Ostinelli, E. G., Zangani, C., Giordano, B., Maestri, D., Gambini, O., D'Agostino, A., . . . Purgato, M. (2021). Depressive symptoms and depression in individuals with internet gaming disorder: A systematic review and meta-analysis. *J Affect Disord, 284*, 136-142. doi:10.1016/j.jad.2021.02.014

Park, H., Yang, J., Vassileva, J., & Ahn, W.-Y. (2021). Development of a novel computational model for the Balloon Analogue Risk Task: The exponential-weight mean–variance model. *Journal of Mathematical Psychology, 102*. doi:10.1016/j.jmp.2021.102532

Park, M., Kim, Y. J., & Choi, J.-S. (2016). PM320. Different Patterns of ERP components in Internet Gaming Disorder and Alcohol Use Disorder: an auditory event-related potential study. *International Journal of Neuropsychopharmacology, 19*(Suppl_1), 14-14. doi:10.1093/ijnp/pyw041.320 %J International Journal of Neuropsychopharmacology

Pedroni, A., Gianotti, L. R., Koenig, T., Lehmann, D., Faber, P., & Knoch, D. (2017). Temporal Characteristics of EEG Microstates Mediate Trial-by-Trial Risk Taking. *Brain Topogr, 30*(1), 149-159. doi:10.1007/s10548-016-0539-6

Qi, X., Du, X., Yang, Y., Du, G., Gao, P., Zhang, Y., . . . Zhang, Q. (2015). Decreased modulation by the risk level on the brain activation during decision making in adolescents with internet gaming disorder. *Front Behav Neurosci, 9*, 296. doi:10.3389/fnbeh.2015.00296

Rilling, J. K., & Sanfey, A. G. (2011). The neuroscience of social decision-making. *Annu Rev Psychol, 62*, 23-48. doi:10.1146/annurev.psych.121208.131647

Sakagami, M., Pan, X., & Uttl, B. (2006). Behavioral inhibition and prefrontal cortex in decision-making. *Neural Netw, 19*(8), 1255-1265. doi:10.1016/j.neunet.2006.05.040

Salehinejad, M. A., Ghanavati, E., Rashid, M. H. A., & Nitsche, M. A. (2021). Hot and cold executive functions in the brain: A prefrontal-cingular network. *Brain Neurosci Adv, 5*, 23982128211007769. doi:10.1177/23982128211007769

Shin, Y. B., Kim, H., Kim, S. J., & Kim, J. J. (2021). A neural mechanism of the relationship between impulsivity and emotion dysregulation in patients with Internet gaming disorder. *Addict Biol, 26*(3), e12916. doi:10.1111/adb.12916

Singh, A. K., Okamoto, M., Dan, H., Jurcak, V., & Dan, I. (2005). Spatial registration of multichannel multi-subject fNIRS data to MNI space without MRI. *Neuroimage, 27*(4), 842-851. doi:10.1016/j.neuroimage.2005.05.019

St. Onge, J. R., & Floresco, S. B. (2009). Prefrontal Cortical Contribution to Risk-Based Decision Making. *Cerebral Cortex, 20*(8), 1816-1828. doi:10.1093/cercor/bhp250 %J Cerebral Cortex

Stevens, M. W., Dorstyn, D., Delfabbro, P. H., & King, D. L. (2021). Global prevalence of gaming disorder: A systematic review and meta-analysis. *Aust N Z J Psychiatry, 55*(6), 553-568. doi:10.1177/0004867420962851

Tom, S. M., Fox, C. R., Trepel, C., & Poldrack, R. A. (2007). The neural basis of loss aversion in decision-making under risk. *Science, 315*(5811), 515-518. doi:10.1126/science.1134239

van Ravenzwaaij, D., Dutilh, G., & Wagenmakers, E.-J. (2011). Cognitive model decomposition of the BART: Assessment and application. *Journal of Mathematical Psychology, 55*(1), 94-105. doi:10.1016/j.jmp.2010.08.010

Vecchio, F., Nucci, L., Pappalettera, C., Miraglia, F., Iacoviello, D., & Rossini, P. M. (2022). Time-frequency analysis of brain activity in response to directional and non-directional visual stimuli: an event related spectral perturbations (ERSP) study. *J Neural Eng, 19*(6). doi:10.1088/1741-2552/ac9c96

Vehtari, A., Gelman, A., & Gabry, J. (2017). Practical Bayesian model evaluation using leave-one-out cross-validation and WAIC. *Statistics and Computing, 27*(5), 1413-1432. doi:10.1007/s11222-016-9696-4

Wagenmakers, E.-J., Farrell, S. J. P. b., & review. (2004). AIC model selection using Akaike weights. *11*(1), 192-196.

Wang, L., Yang, G., Zheng, Y., Li, Z., Qi, Y., Li, Q., & Liu, X. (2021). Enhanced neural responses in specific phases of reward processing in individuals with Internet gaming disorder. *J Behav Addict, 10*(1), 99-111. doi:10.1556/2006.2021.00003

Wang, Y., Cheung, H., Yee, L. T. S., & Tse, C.-Y. (2020). Feedback-related negativity (FRN) and theta oscillations: Different feedback signals for non-conform and conform decisions. *Biological Psychology, 153*, 107880. doi:10.1016/j.biopsycho.2020.107880

Weinstein, A., & Lejoyeux, M. (2020). Neurobiological mechanisms underlying internet gaming disorder *Dialogues Clin Neurosci, 22*(2), 113-126. doi:10.31887/DCNS.2020.22.2/aweinstein

Weinsztok, S., Brassard, S., Balodis, I., Martin, L. E., & Amlung, M. (2021). Delay Discounting in Established and Proposed Behavioral Addictions: A Systematic Review and Meta-Analysis. *Front Behav Neurosci, 15*, 786358. doi:10.3389/fnbeh.2021.786358

Xu, S.-Y., Lu, F.-M., Wang, M.-Y., Hu, Z.-S., Zhang, J., Chen, Z.-Y., . . . Yuan, Z. (2020). Altered Functional Connectivity in the Motor and Prefrontal Cortex for Children With Down's Syndrome: An fNIRS Study. *14*. doi:10.3389/fnhum.2020.00006

Xue, G., Lu, Z., Levin, I. P., & Bechara, A. (2011). An fMRI study of risk-taking following wins and losses: implications for the gambler's fallacy. *Hum Brain Mapp, 32*(2), 271-281. doi:10.1002/hbm.21015

Yao, Y.-W., Zhang, J.-T., Fang, X.-Y., Liu, L., & Potenza, M. N. (2022). Reward-related decision-making deficits in internet gaming disorder: a systematic review and meta-analysis. *Addiction, 117*(1), 19-32. doi:10.1111/add.15518

Yao, Y. W., Chen, P. R., Li, S., Wang, L. J., Zhang, J. T., Yip, S. W., . . . Fang, X. Y. (2015). Decision-making for risky gains and losses among college students with Internet gaming disorder. *PLoS One, 10*(1), e0116471. doi:10.1371/journal.pone.0116471

Yao, Y. W., Wang, L. J., Yip, S. W., Chen, P. R., Li, S., Xu, J., . . . Fang, X. Y. (2015). Impaired decision-making under risk is associated with gaming-specific inhibition deficits among college students with Internet gaming disorder. *Psychiatry Res, 229*(1-2), 302-309. doi:10.1016/j.psychres.2015.07.004

Yau, Y. H., Potenza, M. N., Mayes, L. C., & Crowley, M. J. (2015). Blunted feedback processing during risk-taking in adolescents with features of problematic Internet use. *Addict Behav, 45*, 156-163. doi:10.1016/j.addbeh.2015.01.008

Ye, J. C., Tak, S., Jang, K. E., Jung, J., & Jang, J. J. N. (2009). NIRS-SPM: statistical parametric mapping for near-infrared spectroscopy. *44*(2), 428-447.

Yu, M., Liu, T., & Shi, J. (2020). Food is discounted more steeply than money: Evidence from N2 and P3 responses in delay discounting tasks. *Neuropsychologia, 142*, 107469. doi:10.1016/j.neuropsychologia.2020.107469

Zeng, X., Tang, W., Gao, F., Tang, Z., Zhang, Z., Zhang, J., . . . Yuan, Z. (2023). Behavioral modeling and neuroimaging of impaired risky decision making in patients with chronic musculoskeletal pain. *Neurophotonics, 10*(2), 020901. doi:10.1117/1.NPh.10.2.020901

Zhang, J., Hu, Y., Wang, Z., Wang, M., & Dong, G. H. (2020). Males are more sensitive to reward and less sensitive to loss than females among people with internet gaming disorder: fMRI evidence from a card-guessing task. *BMC Psychiatry, 20*(1), 357. doi:10.1186/s12888-020-02771-1

Zhao, Q., Li, H., Hu, B., Wu, H., & Liu, Q. (2017). Abstinent Heroin Addicts Tend to Take Risks: ERP and Source Localization. *Front Neurosci, 11*, 681. doi:10.3389/fnins.2017.00681

Zhou, R., Myung, J. I., & Pitt, M. A. (2021). The scaled target learning model: Revisiting learning in the balloon analogue risk task. *Cognitive Psychology, 128*, 101407. doi:10.1016/j.cogpsych.2021.101407

Zhou, Y., Yao, M., Fang, S., & Gao, X. (2022). A dual-process perspective to explore decision making in internet gaming disorder: An ERP study of comparison with recreational game users. *Computers in Human Behavior, 128*, 107104. doi:10.1016/j.chb.2021.107104

Zhou, Z., Zhou, H., & Zhu, H. (2016). Working memory, executive function and impulsivity in Internet-addictive disorders: a comparison with pathological gambling. *Acta Neuropsychiatr, 28*(2), 92-100. doi:10.1017/neu.2015.54

Zilverstand, A., Huang, A. S., Alia-Klein, N., & Goldstein, R. Z. (2018). Neuroimaging Impaired Response Inhibition and Salience Attribution in Human Drug Addiction: A Systematic Review. *Neuron, 98*(5), 886-903. doi:10.1016/j.neuron.2018.03.048

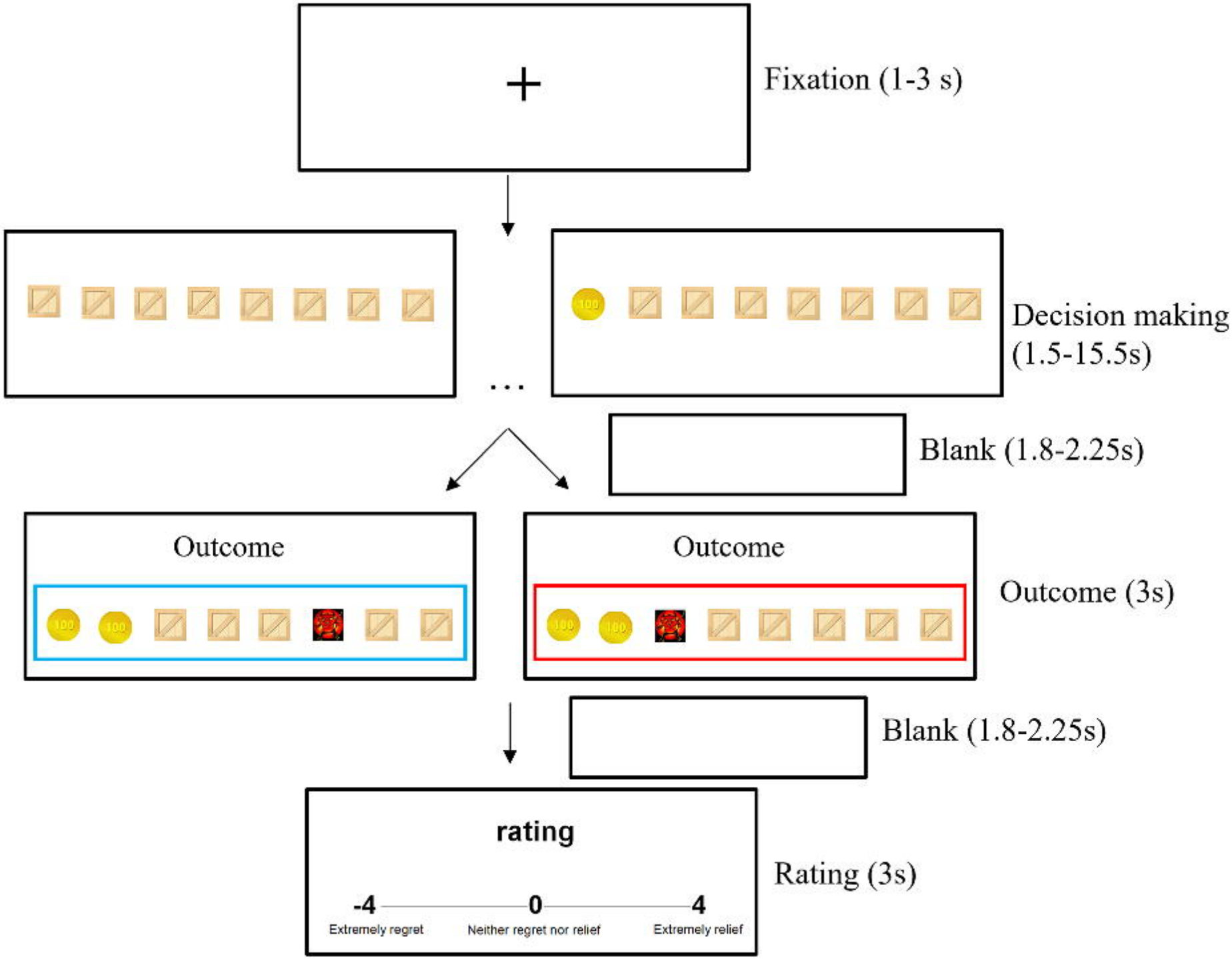
Fixation (1-3 s)
Decision making
(1.5-15.5s)
Blank (1.8-2.25s)
Outcome
Outcome
Outcome (3s)
Blank (1.8-2.25s)
rating
-4
0
4
Extremely regret
Neither regret nor relief
Extremely relief
Rating (3s)

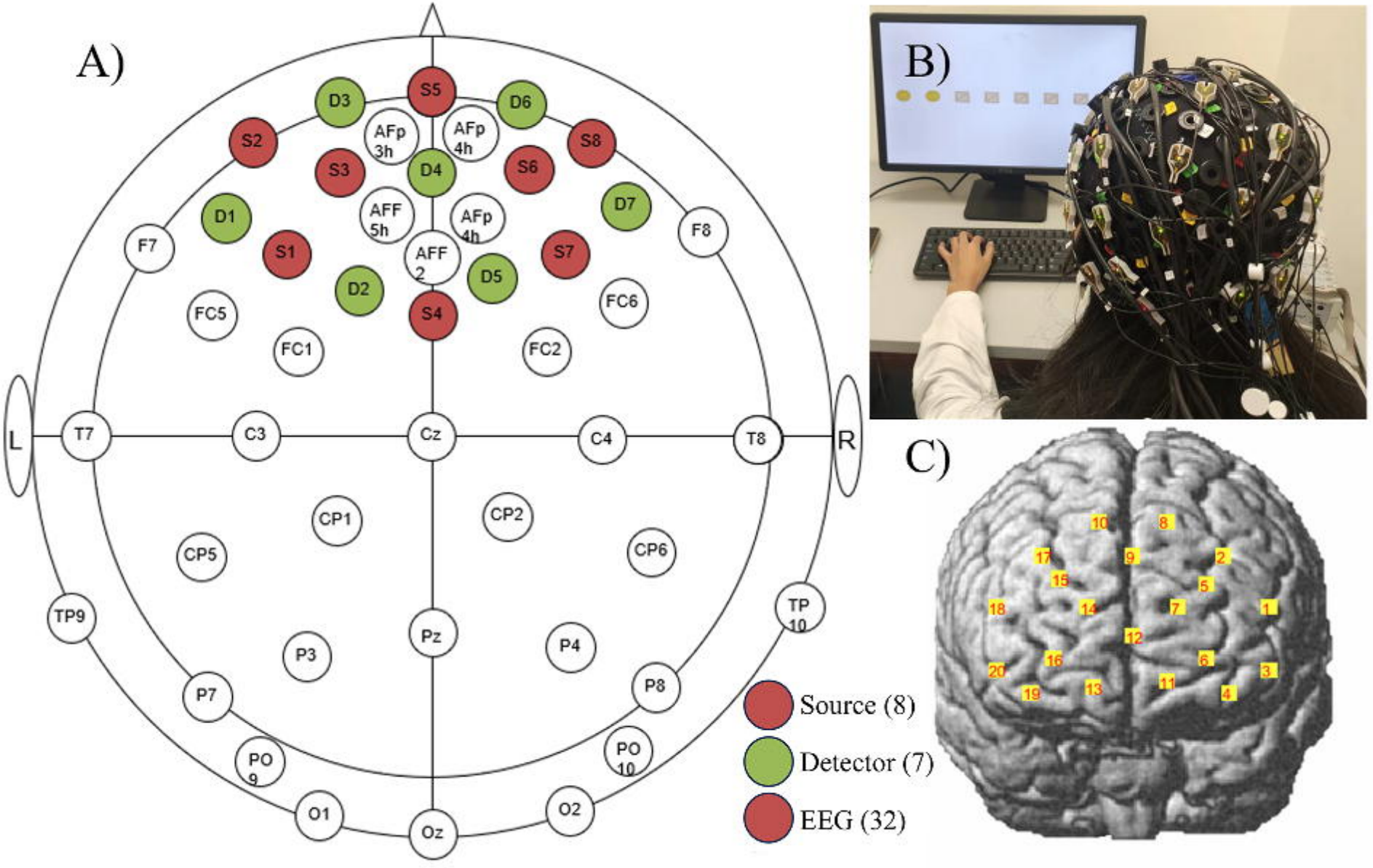
A)
B)
C)
S5
D3
D6
S2
S8
AFp 3h
AFp 4h
S3
D4
S6
D1
D7
AFF 5h
AFp 4h
F7
F8
S1
S7
AFF 2
D2
D5
FC5
FC6
S4
FC1
FC2
L
T7
C3
Cz
C4
T8
R
CP1
CP2
CP5
CP6
TP9
TP 10
Pz
P3
P4
P7
P8
PO 9
PO 10
O1
Oz
O2
Source (8)
Detector (7)
EEG (32)

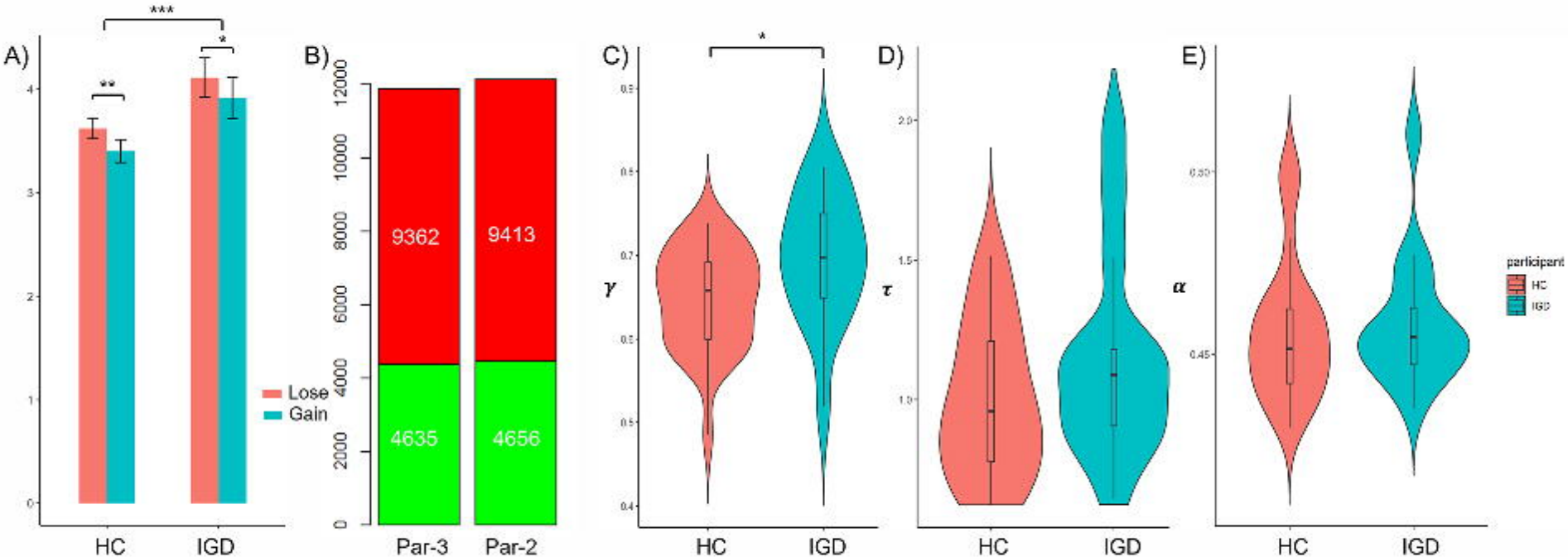
A)
***
**
*
Lose
Gain
HC
IGD
B)
9362
9413
4635
4656
Par-3
Par-2
C)
*
γ
HC
IGD
D)
τ
HC
IGD
E)
α
HC
IGD
participant
HC
IGD

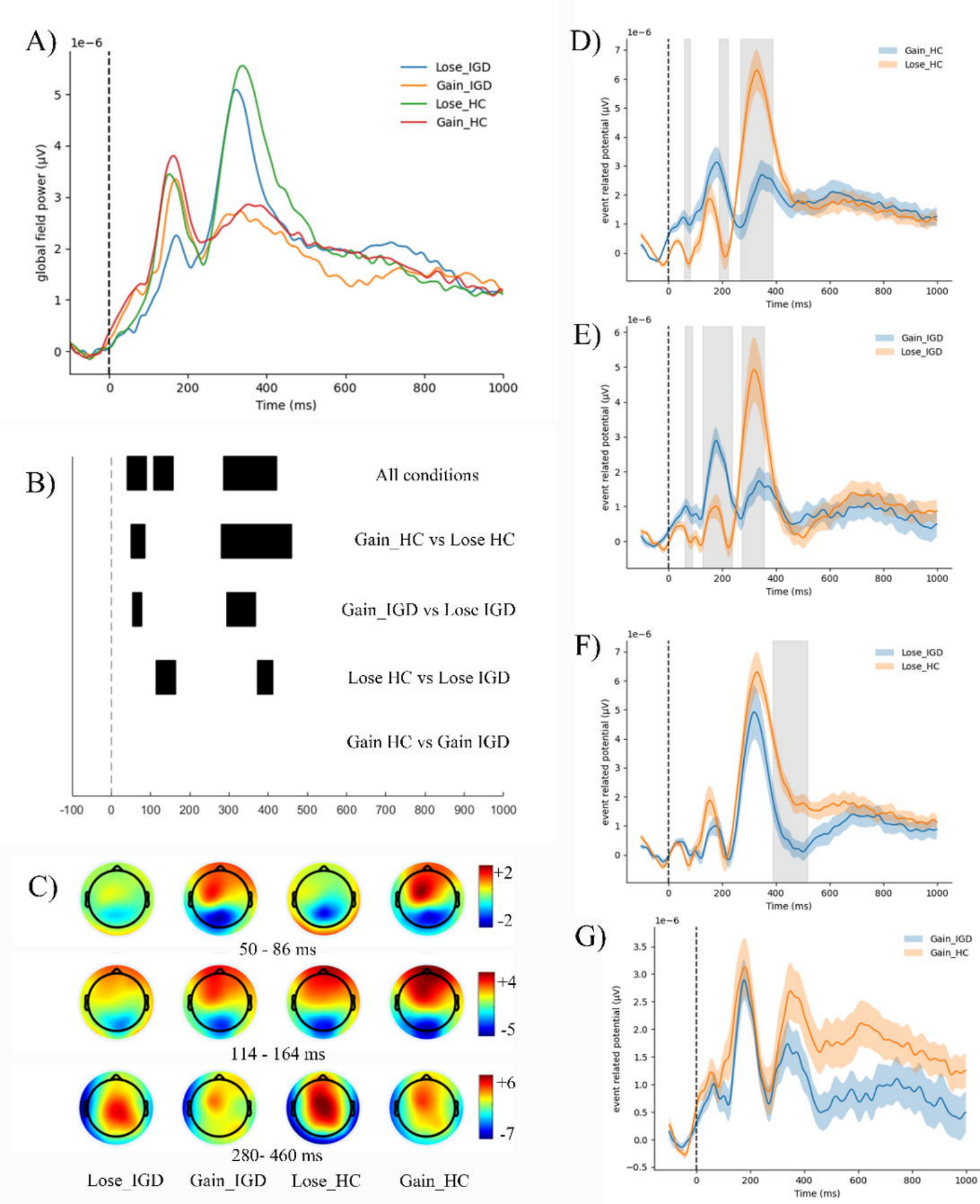
A)
1e−6
global field power (μV)
Time (ms)
Lose_IGD
Gain_IGD
Lose_HC
Gain_HC
B)
All conditions
Gain_HC vs Lose HC
Gain_IGD vs Lose IGD
Lose HC vs Lose IGD
Gain HC vs Gain IGD
C)
50 - 86 ms
114 - 164 ms
280- 460 ms
Lose_IGD
Gain_IGD
Lose_HC
Gain_HC
D)
Gain_HC
Lose_HC
event related potential (μV)
Time (ms)
E)
Gain_IGD
Lose_IGD
F)
Lose_IGD
Lose_HC
G)
Gain_IGD
Gain_HC

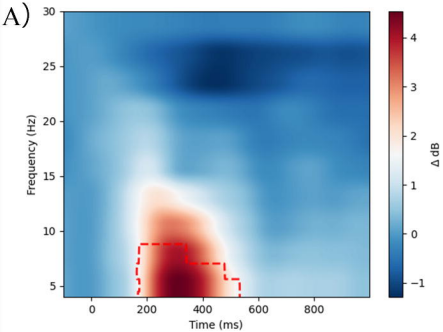
A)
Frequency (Hz)
Time (ms)
Δ dB

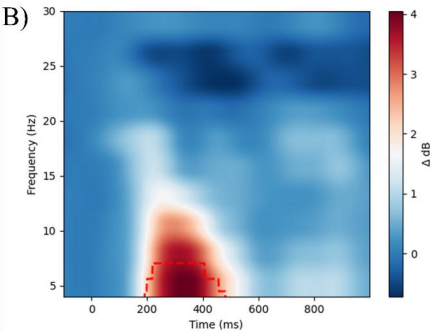
B)
Frequency (Hz)
Time (ms)
Δ dB

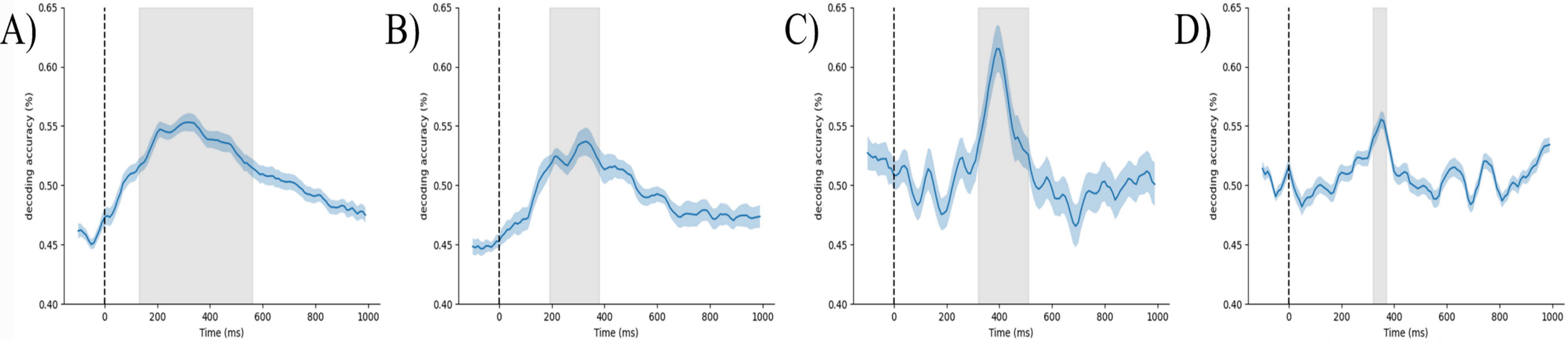

Gain_HC vs Lose_HC

Gain_IGD vs Lose_IGD

Lose_HC vs Lose_IGD

Gain_HC vs Gain_IGD

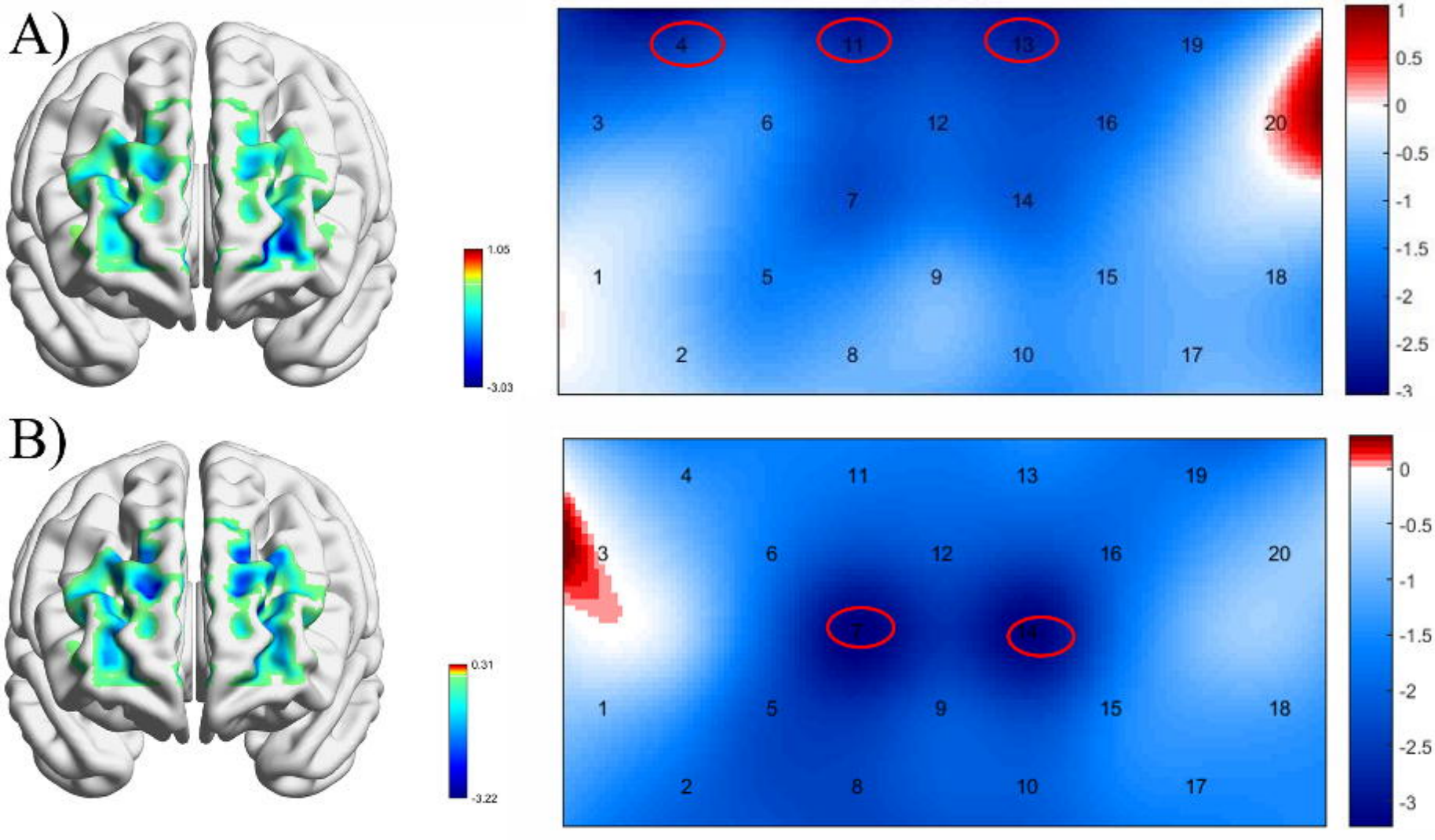
A)
1.05
-3.03
4
11
13
19
3
6
12
16
20
7
14
1
5
9
15
18
2
8
10
17
1
0.5
0
-0.5
-1
-1.5
-2
-2.5
-3
B)
0.31
-3.22
4
11
13
19
3
6
12
16
20
7
14
1
5
9
15
18
2
8
10
17
0
-0.5
-1
-1.5
-2
-2.5
-3

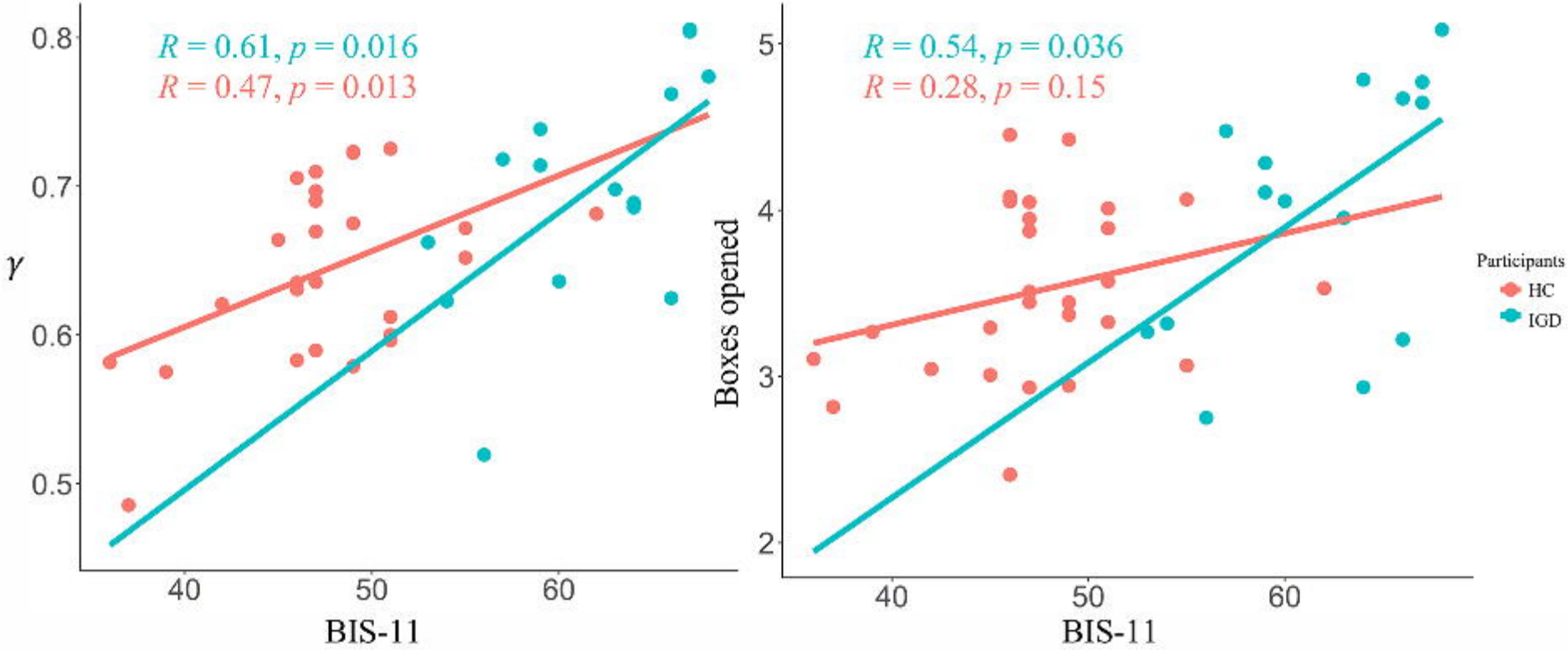
R = 0.61, p = 0.016
R = 0.47, p = 0.013
γ
0.8
0.7
0.6
0.5
40
50
60
BIS-11
R = 0.54, p = 0.036
R = 0.28, p = 0.15
Boxes opened
5
4
3
2
40
50
60
BIS-11
Participants
HC
IGD